

# EROs found behind lensing clusters. II. Stellar populations and dust properties of optical dropout EROs and comparison with related objects <sup>★</sup>

D.Schaerer<sup>1,2</sup>, A.Hempel<sup>1</sup>, E.Egami<sup>3</sup>, R.Pelló<sup>2,4</sup>, J.Richard<sup>2,4</sup>, J.-F. Le Borgne<sup>2</sup>, J.-P. Kneib<sup>5</sup>, M. Wise<sup>6</sup>, and F. Boone<sup>7</sup>

<sup>1</sup> Geneva Observatory, University of Geneva, 51, chemin des Maillettes, CH-1290 Sauverny, Switzerland  
e-mail: daniel.schaerer@obs.unige.ch  
e-mail: angela.hempel@obs.unige.ch

<sup>2</sup> Observatoire Midi-Pyrénées, Laboratoire d'Astrophysique, UMR 5572, 14 Avenue E.Belin, F-31400 Toulouse, France

<sup>3</sup> Steward Observatory, University of Arizona, 933 North Cherry Street, Tucson, AZ 85721, USA

<sup>4</sup> Caltech Astronomy, MC105-24, Pasadena, CA 91125, USA e-mail:

<sup>5</sup> OAMP, Laboratoire d'Astrophysique de Marseille, UMR 6110 traverse du Siphon, F-13012 Marseille, France

<sup>6</sup> Astronomical Institute Anton Pannekoek, Kruislaan 403, NL-1098 SJ Amsterdam, The Netherlands

<sup>7</sup> Observatoire de Paris, LERMA, 61 Av. de l'Observatoire, F-75014 Paris, France

Received 19 january 2007 / Accepted march 2007

## ABSTRACT

**Context.** On the nature, redshift, stellar populations and dust properties of optically faint or non-detected extremely red objects.

**Aims.** We determine the nature, redshift, stellar populations and dust properties of optically faint or non-detected extremely red objects (ERO) found from our survey of the lensing clusters A1835 and AC114 (Richard et al. 2006). Comparison with properties of related galaxies, such as IRAC selected EROs and a  $z \sim 6.5$  post-starburst galaxy candidate from the Hubble Ultra Deep Field.

**Methods.** Using an updated version of *Hyperz* (Bolzonella et al. 2000) and a large number of spectral templates we perform broad-band SED fitting. The photometric observations, taken from Hempel et al. (2007), include deep optical, ACS/HST, ISAAC/VLT, IRAC/Spitzer data, and for some objects also 24  $\mu$ m MIPS/Spitzer and sub-mm data.

**Results.** For most of the lensed EROs we find photometric redshifts showing a strong degeneracy between “low- $z$ ” ( $z \sim 1-3$ ) and high- $z$  ( $z \sim 6-7$ ). Although formally best fits are often found at high- $z$ , their resulting bright absolute magnitudes, the number density of these objects, and in some cases Spitzer photometry or longer wavelength observations, suggest strongly that all of these objects are at “low- $z$ ”. The majority of these objects are best fitted with relatively young ( $\lesssim 0.5-0.7$  Gyr) and dusty starbursts. Three of our objects show indications for strong extinction, with  $A_V \sim 2.4-4$ . The typical stellar masses of our objects are  $M_\star \sim (0.5 - 5) \times 10^{10} M_\odot$  after correction for lensing; for the most extreme ERO in our sample, the sub-mm galaxy SMMJ14009+0252 most likely at  $z_{\text{fit}} \sim 3$ , we estimate  $M_\star \sim 6 \times 10^{11} M_\odot$ . For dusty objects star formation rates (SFR) have been estimated from the bolometric luminosity determined after fitting of semi-empirical starburst, ERO, and ULIRG templates. Typically we find  $\text{SFR} \sim (1 - 18) M_\odot \text{ yr}^{-1}$ . Again, SMMJ14009+0252 stands out as a LIRG with  $\text{SFR} \sim 1000 M_\odot \text{ yr}^{-1}$ . Finally, we predict the mid-IR to sub-mm SED of the dusty objects for comparison with future observations with APEX, Herschel, and ALMA. Concerning the comparison objects, we argue that the massive post-starburst  $z \sim 6.5$  galaxy candidate HUDF-J2 showing observed properties very similar to our EROs, is more likely a dusty starburst at  $z \sim 2.3-2.6$ . This interpretation also naturally explains the observed 24  $\mu$ m emission from this object and we predict its IR to sub-mm SED.

Both empirically and from our SED fits we find that the IRAC selected EROs from Yan et al. (2004) show very similar properties to our lensed EROs. Reasonable fits are found for most of them with relatively young and dusty stellar populations.

**Key words.** Galaxies – high-redshift – evolution – starburst – Cosmology – early Universe – Infrared: galaxies

Send offprint requests to: D.Schaerer

Send offprint requests to: daniel.schaerer@obs.unige.ch

<sup>★</sup> Based on observations collected at the Very Large Telescope (Antu/UT1), European Southern Observatory, Paranal, Chile (ESO Programs 69.A-0508, 70.A-0355, 73.A-0471), the NASA/ESA Hubble Space Telescope obtained at the Space Telescope Science

Institute which is operated by AURA under NASA contract NAS5-26555, the Spitzer Space Telescope, which is operated by the Jet Propulsion Laboratory, California Institute of Technology under NASA contract 1407, and the Chandra satellite.

## 1. Introduction

Various searches for distant galaxies based on a combination of deep broad-band optical and near-IR imaging using the Lyman break technique have been undertaken during the last years, e.g. based on data in the Hubble Ultra Deep Field (HUDF), on the GOODS survey, or others (e.g. Stanway et al. 2003, Yan et al. 2003, Bouwens et al. 2006). Relying on the use of strong gravitational lensing provided by rich foreground galaxy clusters, we have recently undertaken such a pilot program with the main aim of identifying  $z \sim 6$ –10 star forming galaxies (see e.g. Pelló et al. 2004, Richard et al. 2006, and an overview in Schaerer et al. 2006). Such candidates are selected through the now classical Lyman break technique as optical drop-out galaxies showing an intrinsically blue UV restframe colour, as measured from near-IR colours.

As a “by-product” galaxies with red spectral energy distributions (SEDs) are also found among the drop-outs. For example, in the study of two lensing clusters A1835 and AC114 by Richard et al. (2006) we found 8 lensed galaxies with  $R - K_s > 5.6$  and red near-IR colours satisfying one of the often used criteria of “Extremely Red Objects” or EROs. The present paper focuses on these galaxies and related objects, using new ACS/HST observations in the  $z_{850LP}$  band and Spitzer imaging obtained recently and discussed in Hempel et al. (2007, hereafter paper I). Down to the available depth ( $I_{AB} \sim 27.3$  to  $V_{AB} \sim 28$ .) none except one of these objects is detected shortward of  $z_{850LP}$  ( $\lambda_{eff} \sim 9100 \text{ \AA}$ ). This could imply that some of them are red galaxies at very high redshift ( $z \gtrsim 6$ ) or lower redshift objects with a very strong extinction. Quantifying the properties of these EROs and comparing them with similar objects is the main aim of the present work.

Generally speaking, at  $z \gtrsim 1$  EROs are found to be either dusty starbursts or old passive galaxies. They are interesting in their own right and in the context of galaxy formation and evolution (e.g. review by McCarthy 2004). While normally EROs are found at relatively low redshift ( $z \sim 1$ –2), there are attempts to search for similar galaxies at higher  $z$  or for even more extreme – i.e. redder – objects, by selection at longer wavelengths. E.g. Yan et al. (2004) have identified IRAC selected EROs (or IEROs) in the HUDF. In these ultra-deep images the IEROs turn out to be very faint in optical bands ( $\sim 27$ –30 mag in  $V$ ,  $i$  or  $z_{850LP}$ ), such that they could be taken for optical drop-outs in images with less depth. Their redshift has been estimated between  $\sim 1.6$  and 2.9 (Yan et al.). Other selection criteria, such as searches for optical drop-out objects with old populations yield at least partial overlap with EROs, as e.g. demonstrated by the post-starburst  $z \sim 6.5$  galaxy candidate of Mobasher et al. (2005), which also fares among the IEROs just mentioned. Also, a fraction of the sub-mm galaxies, detected through their strong dust emission, show optical to near-IR colours compatible with EROs (cf. e.g. Blain et al. 2002). This is also the case for one of our objects, SMMJ14009+0252, a known lensed sub-mm galaxy which also classifies as an ERO. Finally, optically faint and red objects have also been found by selection of high X-ray to optical fluxes. These so-called EXOs are thought to be AGN at very high redshift ( $z \gtrsim 6$ ) or in very

dusty and/or sub-luminous host galaxies at more moderate redshifts ( $z \sim 2$ –3; see e.g. Koekemoer et al. 2004).

Given this variety of optically faint or undetected and red galaxies it is of interest to determine and compare their properties to clarify their nature, and ultimately to obtain a coherent picture of these seemingly different galaxy populations. With these objectives, we have carried out a detailed quantitative analysis of the stellar populations and dust properties of the lensed EROs found by Richard et al. (2006) benefiting from the new ACS/HST and Spitzer photometry available for these lensing clusters (see paper I). The same SED fitting method, based on the photometric redshift code *Hyperz* (Bolzonella et al. 2000) and using a large set of spectral templates, was also applied to objects with similar SEDs, such as the IRAC selected EROs of Yan et al. (2004) and other objects from the HUDF.

The paper is structured as follows. In Sect. 2 we briefly summarise the observational data for our lensed EROs. The SED fitting method is described in Sect. 3. Results for the SMMJ14009+0252 galaxy are presented and discussed in Sect. 4. The other EROs are discussed in Sect. 5. In Sect. 6 we analyse and discuss the properties of related objects from the HUDF. Our main conclusions are summarised in Sect. 8.

Throughout this paper we adopted the following cosmology:  $\Omega_m = 0.3$ ,  $H_0 = 70 \text{ km s}^{-1} \text{ Mpc}^{-1}$  in a flat universe. Except if mentioned otherwise, all magnitudes are given in the Vega system.

## 2. Observations

The present work deals primarily with the 8 EROs detected as red ( $R - K_s > 5.6$ ) optically non-detected objects in the fields of the lensing clusters A1835 and AC114 by Richard et al. (2006). The images obtained by Richard et al. were complemented with new ACS/HST observations in the  $z_{850LP}$  band (optical), and where possible with Spitzer observations at near-to mid-IR wavelengths (IRAC 3.6, 4.5, 5.8, and 8.0  $\mu\text{m}$ , and MIPS 24  $\mu\text{m}$  photometry).

All details concerning the photometric data reduction are given in Hempel et al. (2007, paper I). The photometry from paper I is summarised in Tables 1, 2, and 3. In this paper the EROs from Richard et al. were reselected from the  $K_s$  band image and optical and near-IR photometry measured with SExtractor using AUTO\_MAG. For the photometry from different instruments source matching was done using object coordinates based on astrometry using the ESO-USNO-A2.0 catalog. For Spitzer total aperture-corrected flux densities were determined from measurements in 3'' diameter apertures. No attempt has been made to correct the differences in flux measurement that are caused by the different apertures and image quality. This is not necessary as we do not use aperture photometry for the optical and near-infrared images, or in case of Spitzer perform aperture correction. The photometry used, AUTO\_MAG, is determined by measuring the flux in a flexible elliptical aperture around each object and accounts for the extended brightness distribution for the brighter objects. Possible differences in the photometry with respect to the earlier measurements of Richard et al. (2006) are discussed in paper I. Using fixed aperture near-IR photometry implies only relatively small changes

**Table 1.** Photometry of the selected ERO subsample in Abell 1835 and AC 114 taken from Hempel et al. (2007, paper I). All magnitudes are given in the Vega system. For conversion to the AB system see the filter properties listed in Table 3. Non-detections (lower limits) are  $1\sigma$  values. NA stands for non available.

| Object    | V     | R     | I     | $z_{850LP}$             | SZ         | J          | H          | Ks          |
|-----------|-------|-------|-------|-------------------------|------------|------------|------------|-------------|
| A1835-#1  | >28.1 | >27.8 | >26.7 | 25.70±0.07              | 24.44±0.27 | 22.76±0.16 | 22.40±0.08 | 20.74±0.02  |
| A1835-#2  | >28.1 | >27.8 | >26.7 | >27.46                  | 24.08±0.26 | 24.41±1.34 | 21.78±0.06 | 20.45±0.02  |
| A1835-#3  | >28.1 | >27.8 | >26.7 | 24.06±0.07 <sup>a</sup> | 23.78±0.10 | 24.32±0.47 | 22.55±0.07 | 21.58±0.03  |
| A1835-#4  | >28.1 | >27.8 | >26.7 | 25.48±0.14              | 24.44±0.15 | 23.56±0.18 | 22.90±0.07 | 21.95±0.03  |
| A1835-#10 | >28.1 | >27.8 | >26.7 | 25.56±0.11              | 24.00±0.12 | 23.72±0.26 | 23.36±0.13 | 21.67±0.03  |
| A1835-#11 | >28.1 | >27.8 | >26.7 | >27.46                  | >26.9      | 23.92±0.37 | 23.49±0.18 | 21.29±0.03  |
| A1835-#17 | >28.1 | >27.8 | >26.7 | >27.46                  | >26.9      | > 25.6     | 23.51±0.16 | 22.11±0.03  |
| AC114-#1  | >28.5 | >27.7 | >26.8 | 24.55±0.07              | NA         | 21.26±0.04 | 19.75±0.01 | 18.62±0.001 |

<sup>a</sup> This source appears double in the  $z_{850LP}$  image. The fainter component has 25.31±0.07. In the SED modeling the brighter magnitude or the sum of two have been used.

**Table 2.** IRAC and MIPS 24  $\mu$ m photometry of the EROs listed in Table 1 taken from paper I. All fluxes are given in  $\mu$ Jy. Upper limits are 1-sigma noise values at the position of the sources. Due to source blending the data is uncomplete, i.e. not available for objects A1835-#3, A1835-#10, and A1835-#11, and partially for A1835-#1.

| Object    | IRAC/Spitzer |            |            |            | MIPS        |
|-----------|--------------|------------|------------|------------|-------------|
|           | 3.6          | 4.5        | 5.8        | 8.0        | 24.0        |
| A1835-#1  | 2.9 ± 0.2    | 4.0 ± 0.2  | blended    |            | < 10        |
| A1835-#2  | 14.4 ± 0.2   | 23.3 ± 0.3 | 37.6 ± 1.5 | 50.9 ± 1.6 | 320 ± 11    |
| A1835-#4  | 1.9 ± 0.2    | 1.0 ± 0.3  | < 0.7      | < 0.6      | < 10        |
| A1835-#17 | 2.4 ± 0.2    | 1.6 ± 0.2  | < 0.6      | < 0.5      | < 10        |
| AC114-#1  | 67.3 ± 0.5   | 64.4 ± 0.5 | 50.3 ± 1.5 | 44.9 ± 2.2 | 189.0 ± 8.9 |

and does not alter our overall conclusions, as test computations have shown. The new measurements, adapted to the morphology of the EROs, are used in the present paper. In the SED modeling discussed below we consider also a minimum photometric error to account for uncertainties due to matching photometry from different instruments.

No object from the subsample of “optical dropout” EROs discussed in paper I is detected shortward of the *R* band. For modeling in the present work we include the *V* band non-detection as the dropout constraint. Non-detections at shorter wavelengths are redundant and are therefore not included in the SED fitting.

An overview of the observed optical, near-IR, and IRAC/Spitzer fluxes of all the objects discussed in this paper is shown in Fig. 1.

### 3. SED fitting method

An SED fitting technique based on an updated version of the *Hyperz* code from Bolzonella et al. (2000) is used to constrain the redshift, stellar population properties (age, star formation history), and extinction of the galaxies studied in this paper. To do so we closely follow the procedures outlined in Schaerer & Pelló (2005). In addition we have included other synthetic, empirical and semi-empirical spectral templates, as described below.

#### 3.1. Photometry

Ground-based, HST, and Spitzer photometry of the lensed EROs is taken from paper I. The following bands have been included in the SED fitting: *V*, *R*, *I* nondetections,  $z_{850LP}$  from ACS/HST, *SZ*, *J*, *H*, *Ks* from ISAAC/VLT, channels 1–4 from IRAC/Spitzer and 24  $\mu$ m MIPS/Spitzer where available. The filter properties are listed in Table 3.

For other objects, included here for comparison, the original photometry was taken from the literature.

In some cases a prescribed minimum photometric error is assumed, to examine the influence of possibly underestimated error bars and to account for uncertainties in absolute flux calibrations when combining photometry from different instruments.

#### 3.2. Spectral templates

The following spectral templates, assembled into several groups, have been used in the fit procedure.

- **Bruzual & Charlot** plus Coleman et al. (1980) empirical templates galaxies of all Hubble types (hereafter named BC or BCCWW group). The theoretical Bruzual & Charlot (2001) models, taken here for solar metallicity, include various star formation histories representative of different Hubble types (burst, and e-folding times of  $\tau=1, 2, 3, 5, 15, 30$ , and  $\infty$  Gyr corresponding to E, S0, Sa, Sb, Sc, Sd,

**Table 3.** Properties of the photometric filters used for the SED fitting of objects in the field of A1835 and of AC114. For AC114 alternate filters are listed in parenthesis and SZ observations are not available (entry NA). Col. 1 indicates the filter name, col. 2 the effective wavelength in micron, col. 3 the effective bandpass (filter “width”) in micron computed with a Gaussian approximation. AB corrections ( $C_{AB}$ ), defined by  $m_{AB} = m_{Vega} + C_{AB}$ , are listed in col. 3. Detailed information on the photometry can be found in paper I.

| Filter                | $\lambda_{eff}$ [ $\mu m$ ] | $\Delta\lambda$ [ $\mu m$ ] | $C_{AB}$      |
|-----------------------|-----------------------------|-----------------------------|---------------|
| V                     | 0.543                       | 0.056                       | 0.018         |
| R (R <sub>702</sub> ) | 0.664 (0.700)               | 0.075 (0.123)               | 0.246 (0.299) |
| I (I <sub>814</sub> ) | 0.817 (0.807)               | 0.117 (0.137)               | 0.462 (0.445) |
| Z <sub>850LP</sub>    | 0.911                       | 0.114                       | 0.540         |
| SZ (NA)               | 1.070                       | 0.094                       | 0.698         |
| J                     | 1.259                       | 0.167                       | 0.945         |
| H                     | 1.656                       | 0.180                       | 1.412         |
| Ks                    | 2.165                       | 0.181                       | 1.871         |
| IRAC 3.6 $\mu m$      | 3.577                       | 0.427                       | 2.790         |
| IRAC 4.5 $\mu m$      | 4.530                       | 0.567                       | 3.249         |
| IRAC 5.8 $\mu m$      | 5.788                       | 0.801                       | 3.737         |
| IRAC 8.0 $\mu m$      | 8.045                       | 1.634                       | 4.392         |

and Im types). The IMF adopted in these models is the Miller-Scalo IMF from 0.1 to 125  $M_{\odot}$ . We have not included the templates from the Bruzual & Charlot (2003) update, as this concerns mostly high resolution spectral libraries which have no impact on our results.

- **Starburst SEDs from Schaerer** (2002, 2003) models at different metallicities extended up to ages of 1 Gyr and considering instantaneous bursts or constant star formation (s04gyr group). The overall SEDs predicted by these synthesis models, including in particular nebular continuum emission neglected in the Bruzual & Charlot models, are basically identical to the ones from *Starburst99* (Leitherer et al. 1999). However, a larger variety of metallicities is included. These models assume a Salpeter IMF from 1 to 100  $M_{\odot}$ .
- **Maraston models** (Maraston 2005) including a semi-empirical treatment of thermally pulsating AGB stars, whose contribution in the near-IR may be significant in certain phases. This non-standard approach may therefore lead to different age and stellar mass estimates than other synthesis codes (see Maraston 2005 details). The templates used here include simple stellar populations (bursts) with ages up to 15 Gyr, and exponentially decreasing star formation histories with e-folding times up to 2 Gyr.
- **Empirical or semi-empirical starburst, ULIRG and QSO templates.** In addition to starburst templates from the Calzetti et al. (1994) and Kinney et al. (1996) atlas included in the public *Hyperz* version, we have added the HST QSO template of Zheng et al. (1997), and templates of metal-poor H II galaxies SBS0335-052 and Tol 1914-266 including numerous strong emission lines (Izotov private communication).

To include also more obscured objects we have added UV to millimeter band templates of EROs, ULIRGS, star-

burst and normal galaxies (HR 10, Arp 220, M82, NGC 6090, M51, M100, NGC 6949) from fits of GRASIL models to multi-wavelength observations (Silva et al. 1998, named GRASIL group). These templates are therefore semi-empirical templates. This template group will be used in particular to predict mid-IR to sub-mm fluxes, and hence to estimated total bolometric luminosities, after fitting the optical to 8  $\mu m$  part of the spectrum.

### 3.3. Fit procedure and determined parameters

The main free parameters we consider are: the spectral template (among a group), redshift  $z$ , and (additional) extinction ( $A_V$ ) assuming a Calzetti et al. (2000) law. In our standard calculations  $z$  is varied from 0 to 10, and  $A_V$  from 0 to 4 mag. For test purposes higher values of  $A_V$  and other extinction laws are also allowed.

To increase the diversity of empirical or semi-empirical templates and to allow for possible deviations from them, reddening is optionally also considered as a free parameter. In this case, this obviously corresponds to an additional reddening. Test computations have shown an excellent consistency between photometric and spectroscopic redshifts using e.g. the GRASIL template group to fit the near-IR to IRAC observations of Stern et al. (2006) of the ERO HR10, once allowing for possible additional reddening. A similar approach with empirical templates was also adopted by Rigby et al. (2005). As for all templates the corresponding dust emission is not treated consistently.

Finally, from the luminosity distance of the object the scaling of the template SED to the observed absolute fluxes yields an absolute scaling property, such as the stellar mass or the star formation rate (SFR) when templates generated by evolutionary synthesis models are used.

To estimate stellar masses we use two different approaches. 1) We determine the restframe absolute K band magnitude  $M_K^{rest}(Ks)$  from *Hyperz* and assume a typical light-to-mass ratio ( $L_K/M$ ). The stellar mass is then determined as:

$$M_{\star} = 10^{-0.4[M_K^{rest}(Ks) - 3.3]} / (L_K/M) \quad (1)$$

in solar units. The numerical value 3.3 is the solar absolute Ks band magnitude. This approach is applicable to any template, theoretical or empirical ones. For comparison with other dusty galaxies, we adopt the value  $L_K/M = 3.2$  used for SCUBA galaxies by Borys et al. (2005).

2) When using templates from evolutionary synthesis models, the stellar mass (and/or SFR) can be determined from the absolute scaling of the best fit template to the observed fluxes and to the best fit redshift. Note that the Bruzual & Charlot models used here assume a Miller-Scalo IMF from 0.1 to 125  $M_{\odot}$ , whereas the S04 models assume a Salpeter IMF from 1 to 100  $M_{\odot}$ .

The star formation rate is a natural quantity when star formation over a certain time scale (or at a constant rate) is considered. This quantity can therefore only be determined through SED fits using theoretical templates assuming constant star formation. Alternatively, for objects with good fits using the multi-wavelength GRASIL templates covering the restframe UV to

sub-mm domain, we will determine SFRs from the total bolometric luminosity derived over the available spectral range and applying a standard Kennicutt (1998) relation between  $L_{\text{bol}}$  and SFR.

Absolute quantities such as the stellar mass, SFR, and bolometric luminosity depending on the luminosity distance must also be corrected for the effects of gravitational lensing. The magnification factor of each source was determined using the mass models of A1835 (similar to Smith et al. 2005) and AC114 (Natarajan et al. 1998, Campusano et al. 2001), following the same procedure as in Richard et al. (2006). Because of the slight dependence of the magnification with the source redshift  $z_s$ , at the location of the EROs, we computed different estimates assuming  $z_s = 0.5, 1, 2, 3$ , as well as 7 for comparison. The different values, given in Table 4 for each object, reflect the uncertainty in the magnification factor, the source redshift being the dominant source of error. In any case, for the bulk of these sources located somewhat away from the cluster center (see Figs. 10, 11 in Richard et al.), the magnification is relatively small.

**Table 4.** Magnification factors  $\mu$  from the lensing models of A1835 and AC114 predicted for various source redshifts  $z_s$ . The values of  $\mu$  are dimensionless magnification factors, and not in magnitudes.

| Object    | $z_s = 0.5$ | $z_s = 1.$ | $z_s = 2.$ | $z_s = 3.$ | $z_s = 7.$ |
|-----------|-------------|------------|------------|------------|------------|
| A1835-#1  | 1.13        | 1.21       | 1.26       | 1.28       | 1.33       |
| A1835-#2  | 1.38        | 1.71       | 1.95       | 2.05       | 2.32       |
| A1835-#3  | 1.24        | 1.43       | 1.54       | 1.59       | 1.72       |
| A1835-#4  | 1.25        | 1.45       | 1.57       | 1.62       | 1.76       |
| A1835-#10 | 1.19        | 1.33       | 1.42       | 1.45       | 1.54       |
| A1835-#11 | 1.14        | 1.23       | 1.28       | 1.30       | 1.35       |
| A1835-#17 | 1.14        | 1.23       | 1.28       | 1.30       | 1.36       |
| AC114-#1  | 1.49        | 2.24       | 2.87       | 3.15       | 4.03       |

#### 4. The sub-mm galaxy A1835 - #2 (SMMJ14009+0252)

As already mentioned in Richard et al. (2006), this ERO corresponds to the known sub-mm source SMMJ14009+0252 (Ivison et al. 2000, Smail et al. 2002, Frayer et al. 2004). With AC114-#1 this object is the brightest optical dropout ERO from our sample.

##### 4.1. SED fitting results

The observed SED shows, in  $F_\nu$  units (cf. Fig. 4), a continuously increasing SED from the near-IR, through the 4 IRAC channels and up to  $24 \mu\text{m}$  (MIPS), where this object is also detected. When all IRAC bands are included in fits, the solutions with the “standard” templates are driven to high- $z$  ( $z_{\text{phot}}$  between 6 and 8). However, a reasonably low  $\chi^2$  is achieved for all redshifts  $z_{\text{phot}} \gtrsim 3$ ; see  $\chi^2$  map on Fig. 2. For all redshifts a very large extinction ( $A_V \sim 3\text{--}4!$ ) is found as a best fit.

As shown in Figs. 3 and 4, the high- $z$  solution ( $z_{\text{fit}}=7.46$ ) provides an excellent fit to the observed SED. This template

corresponds to a young burst (6 Myr) + high  $A_V$ . The best fit with GRASIL templates is obtained at  $z_{\text{fit}}=2.78$  with the NGC 6090 template plus additional extinction of  $A_V=1.4$ . Imposing a maximum redshift of 4 to the BCCWW templates, one finds a very similar best photometric redshift ( $z_{\text{fit}}=2.95$ ) for an elliptical with 0.36 Gyr plus 2.4 mag extinction in  $A_V$ . These two  $z \sim 3$  solutions are also plotted in Fig. 3, showing a discrepancy at  $\sim 0.95\text{--}1.1 \mu\text{m}$  (cf. below).

Actually the overall SED of this object, including in particular our MIPS  $24 \mu\text{m}$  and the SCUBA measurements from Ivison et al. (2000), is rather well fitted with semi-empirical templates from GRASIL for redshifts  $z \sim 2.8\text{--}3.$ , as shown on Fig. 4. Templates with very strong dust emission such as Arp 220 are needed to reproduce the observed ratio of the sub-mm to near/mid-IR flux. For example, templates of more moderate starbursts like M82 and NGC 6090 underpredict the sub-mm emission. The *Hyperz* best fit with the Arp 220 template requires an additional extinction of  $A_V = 1.4$  (for the Calzetti et al. law). The only difficulty with fits at  $z_{\text{fit}} \sim 3$  is the excess emission observed in the SZ band, which is  $\sim 5\sigma$  above the expected level at such redshift. A natural explanation could be the Mg II  $\lambda 2798$  emission line seen in type 1 AGNs (e.g. Gavignaud et al. 2006).

Already from the observed monotonous flux increase observed across all 4 IRAC bands it is quite clear that this source cannot be at redshift much smaller than  $\sim 3$ . Otherwise the typical flux depression, associated to the transition from the stellar peak at  $1.6 \mu\text{m}$  (restframe) to the raising dust emission at longer wavelengths (cf. John 1998, Sawicki 2002) should be seen. Excluding higher redshift solutions from the near-IR to  $8 \mu\text{m}$  data used here for the *Hyperz* SED fitting is difficult, and would require a more complex stellar population plus dust modeling. However, if at  $z \sim 6\text{--}8$  as suggested from the formal best fits, the absolute magnitude of this object would be rather exceptional ( $M^{\text{rest}}(K_s) \sim -29.6$  or  $M^{\text{rest}}(V) \sim -26.6$  without correcting for lensing), rendering this case very unlikely. Furthermore radio and sub-mm data (cf. below) as well as our “global” SED analysis favour  $z \ll 6$ . For these various reasons we conclude that the most likely redshift of this object is  $z \sim 3$ . This redshift is larger than the estimate based on the radio-submm spectral index  $\alpha_{1.4}^{850}$ , but in agreement with the one from submm colours (cf. Ivison et al. 2000). It is also larger than our previous estimate based on optical to near-IR photometry (Richard et al. 2006).

Assuming  $z \sim 3$  and a magnification factor  $\mu = 2$  (cf. Table 4) one obtains the following estimates: with a rest-frame absolute magnitude  $M^{\text{rest}}(K_s) \sim -27.7$  this object is  $\sim 3.4$  to  $3.6$  magnitudes brighter than  $M_\star$  at this redshift (cf. Kashikawa et al. 2003) or than  $M_\star(K_s)$  from 2MASS in the local Universe (cf. Kochanek et al. 2001).

The mass, estimated from the best fitting Bruzual & Charlot and S04 templates (with an age of  $\sim 0.36$  and  $0.14$  Gyr respectively), is  $M_\star \sim 1.2 \times 10^{12} / \mu M_\odot$ <sup>1</sup>, slightly more massive e.g. than the most massive SCUBA galaxy discussed by Borys et al. (2005) and typically an order of magnitude more massive than

<sup>1</sup> For the value  $L_K/M = 3.2$  adopted for SCUBA galaxies (cf. Borys et al. 2005) one obtains  $M_\star \sim 7.8 \times 10^{11} / \mu M_\odot$

the most massive  $z \sim 3$  Lyman break galaxy observed with Spitzer by Rigopoulou et al. (2006).

Integrating the global SED of Arp 220 adjusted to the observations (see Fig. 4) and assuming  $z = 2.78$  one obtains a total luminosity of  $L_{\text{bol}} \sim 1.2 \times 10^{13} / \mu L_{\odot}$ , close to the limit between ultra-luminous and hyper-luminous infrared galaxies (ULIRG and HyLIRG). Using standard SFR conversion factors (Kennicutt 1998) this corresponds to an estimated star  $SFR \sim 1050 M_{\odot} \text{ yr}^{-1}$ , adopting  $\mu \sim 2$  (Table 4).

#### 4.2. Discussion

The radio-submm spectral index  $\alpha_{1.4}^{850} = 0.60 \pm 0.03$  indicates a likely redshift of  $0.7 \lesssim z \lesssim 2.3$  (Smail et al. 2000, Ivison et al. 2000). From the 450- to 850- $\mu\text{m}$  flux a coarse estimate of  $z \gtrsim 2.8$  has been derived by Hughes et al. (1998). From the near-IR to submm SED and from the low value of  $\alpha_{1.4}^{850}$ , Ivison et al. (2000) argue that A1835-#2 is more likely at  $3 \lesssim z \lesssim 5$  and that the radio flux contains some AGN contribution. A recent reanalysis of the radio and submm flux by Aretxaga et al. (2003) yields a higher redshift estimate of  $z \sim 4.1 \pm 0.8$ . However, their best fit SED strongly overpredicts the observed near- to mid-IR flux. Our earlier photometric redshift estimate of  $z \sim 1.2\text{--}1.6$  (Richard et al. 2006) is now superseded by the present analysis including in particular the longer wavelength IRAC/Spitzer observations leading to a higher  $z$ . The various redshift estimates, including the one presented here, can be reconciled if the radio flux contains a contribution from an AGN, as already pointed out by Ivison et al. (2000). For our best redshift,  $z \sim 3$ , the AGN contribution does not need to be strong, as also discussed by these authors. As already noted above, the observed SZ band excess could also be an indication for an AGN.

At the high luminosities of this object, in the ULIRG range, the AGN fraction is high ( $\gtrsim 40\text{--}50\%$ , cf. Veilleux et al. 1999, Alexander et al. 2004) rendering the AGN hypothesis quite likely. However, is there other direct evidence for an AGN? Ivison et al. (2000) have obtained an upper limit in soft X-rays (0.1–2.0 keV) from ROSAT archival HRI observations. In our recent Chandra observations of Abell 1835, described in paper I, this object remains undetected with flux limits of the order of  $< (2. - 3.) \times 10^{-16} \text{ erg s}^{-1} \text{ cm}^{-2}$  in the 0.5–7.0 keV band, for photon power law index  $\Gamma$  between 1.0 and 2.0. The corresponding limit for 2.0–10.0 keV and  $\Gamma = 1.4$  is  $\lesssim 2.5 \times 10^{-16} \text{ erg s}^{-1} \text{ cm}^{-2}$ . A comparison with the X-ray and 24  $\mu\text{m}$  fluxes of starbursts and AGN compiled by Alonso-Herrero et al. (2004) places this X-ray limit well below the typical range of hard X-ray selected AGN. A more detailed analysis will be needed to examine how much room these new constraints leave for a putative AGN in this object.

Compared to other SCUBA galaxies studied also in the rest-frame optical (cf. Smail et al. 2004) A1835-#2 fares among the faintest ones in  $K$  and among the “reddest ones” in optical/IR flux. With  $m(Ks) \sim 20.5$  it is close to the faintest objects of Smail et al., which have  $18 \lesssim Ks \lesssim 20.9$ ; among the 7 confirmed sub-mm galaxies observed in the SCUBA Cluster Lens Survey of Frayer et al. (2004) it is the second

faintest object in  $K$  surpassed only by SMMJ00266+1708 with  $m(K) = 22.36 \pm 0.16$ , and the second reddest in  $J - K$ . After lensing correction the magnitude of A1835-#2 is  $m(Ks) \sim 21.2$ . Several other sub-mm galaxies are known with very faint flux levels at  $K \gtrsim 21.0\text{--}21.9$  (Smail et al. 2002, Dannerbauer et al. 2002). Its restframe V-band to IR luminosity ratio is very low,  $\sim 5. \times 10^{-4}$ , placing it among the 5 most extreme sub-mm galaxies when compared to the Smail et al. (2004) sample.

In terms of stellar populations we find a dominant stellar age of  $\sim 0.36$  Gyr or younger for A1835-#2, similar to the mean ages of  $\sim (310 - 530) \pm (80 - 90)$  Myr estimated by Smail et al. (2004) for a sample of sub-mm galaxies and optically faint radio galaxies. The extinction we estimate ( $A_V \sim 2.4\text{--}3$ ) is somewhat larger than the average of  $A_V \sim (1.70\text{--}2.44) \pm (0.13\text{--}0.14)$  found by Smail et al., but comparable to the median  $A_V \sim 2.9 \pm 0.5$  determined by Takata et al. (2006) for sub-mm galaxies from the Balmer decrement. The best fit with the Arp 220 spectrum, requiring an additional extinction of  $A_V = 1.4$ , also indicates that we’re dealing with an object with a rather exceptionally large extinction!

We note also that the stellar mass estimated from the SED fit ( $M_{\star} \sim 1.2 \times 10^{12} / \mu M_{\odot}$ ) is consistent with the mass being built up at the high SFR of  $\sim 2100 / \mu M_{\odot} \text{ yr}^{-1}$  over a period of  $\lesssim 360$  Myr. This leaves room for  $\sim 25\%$  of the stellar mass being formed from a previous star formation event.

### 5. SED fitting results for other objects

We now present the results from the SED fits for the individual objects. First we discuss in detail the objects for which Spitzer photometry (detections or upper limits) is available. The remaining objects are addressed in Sect. 5.5. The main results are summarised in Table 5 and 6. The magnification factors  $\mu$  needed to correct for gravitational lensing are listed in Table 4.

#### 5.1. A1835 - #1

Overall SED fits for this object are rather degenerate and of poor quality (high  $\chi^2$ ), showing several minima for its photometric redshift, most of them at  $z \lesssim 3$  (see Fig. 5). Formally, all template groups yield a  $\chi^2$  minimum at  $z_{\text{fit}} \sim 0.4$ . However, the best fits are of lower quality (higher  $\chi^2$ ) than for the other objects, since the photometry yields an apparently somewhat “non-monotonic” SED. Furthermore the photometric redshift is only loosely constrained as no IRAC photometry is available for channels 3 and 4 (5.8 and 8.0  $\mu\text{m}$ ) due to blending with other sources.

There is a strong degeneracy in this case between redshift and extinction (Fig. 5). Two different solutions coexist, one at  $z_{\text{fit}} \sim 0.4$  and  $A_V \gtrsim 3.4$ , and another one at  $z_{\text{fit}} \sim 1.5$  with  $A_V \leq 1.2$ . The first solution is strongly degenerate in the age- $A_V$  plane as well, thus providing loose constraints on the stellar mass: the stellar ages vary quite strongly from  $\sim 2.3$  Gyr (BC models) to  $\sim 10$  Myr for the Maraston and S04gyr models, and the corresponding stellar masses range from  $\sim 1. \times 10^{10} / \mu M_{\odot}$  (BC) to  $(0.4 - 1.1) \times 10^8 / \mu M_{\odot}$ . Even if we consider the solutions around  $z \sim 1.5$  there are significant uncertainties. E.g. the BC and Maraston models require little extinction ( $A_V \sim 0.6$ ),

whereas S04gyr and GRASIL templates indicate a higher extinction (even  $A_V \sim 3.8$  for S04gyr!). Stellar ages of  $\sim 5.5$  Gyr (1 Gyr) are found for the BC and Maraston (S04gyr) models; the corresponding stellar mass is estimated as  $\sim 8. \times 10^{10} \mu M_\odot$ . For the S04gyr models one obtains  $M_\star \sim 6.3 \times 10^{11} \mu M_\odot$ .

For illustration we show several SED fits including with the semi-empirical GRASIL templates in Fig. 6. The latter allow us in particular to estimate the mid-IR to sub-mm flux. In particular we note that the  $24 \mu\text{m}$  non-detection probably rules out the very dusty solution at  $z \sim 0.4$ , rendering  $z \sim 1.5$  more likely. However, for this object it is clear that the uncertainties on all derived parameters are large, and larger than for the other objects discussed here. For this reason the entries in Table 5 are left blank for this object. For comparison we note that the empirical classification based on near-IR colours would indicate an “old passive” object (paper I).

## 5.2. A1835 - #4

For this object the best fits are consistently found at low redshifts,  $z_{\text{fit}} \sim 1.2$  well constrained by the measurement of the stellar  $1.6 \mu\text{m}$  peak measured in the IRAC channels. The corresponding  $\chi^2$  maps and the best fit SEDs for this object are shown in Figs. 7 and 8.

Best fit templates correspond to bursts of  $\sim 4.5$  Gyr with no extinction for Bruzual & Charlot models or to the elliptical template from CWW, i.e. an old and dust-free galaxy. With the S04 templates the best fit is of similar quality, yielding a younger burst age ( $\sim 0.6$  Gyr) and some extinction ( $A_V \sim 1.6$ ). From the BC and S04 model sets the estimated mass is  $M_\star \sim (1.1 - 1.7) \times 10^{10} / \mu M_\odot$ , with the magnification factor  $\mu \sim 1.5$  (cf. Table 4). If we assume  $L_K/M = 3.2$  as for SCUBA galaxies (cf. Borys et al. 2005), one obtains  $M = 9.4 \times 10^9 / \mu M_\odot$ . For this object SED fits with Maraston models yield a solution of similar quality, but a lower redshift of  $z_{\text{fit}} \sim 0.8$ . The other fit parameters a burst age of 1.7 Gyr,  $A_V = 1.2$ , and a stellar mass of  $4.8 \times 10^9 / \mu M_\odot$ .

For comparison the best fit to GRASIL templates is found at  $z_{\text{fit}} = 1.24$  with an M82 template (and no additional extinction), as shown in Fig. 8. Although the quality of this fit is less than the ones mentioned above, we cannot completely rule out the presence of dust. Observations at longer wavelengths would be needed. Assuming that the M82 template is valid, we estimate a bolometric luminosity of to  $L_{\text{bol}} \sim 2.6 \times 10^{10} / \mu L_\odot$  or a star formation rate of just  $SFR \sim 5 / \mu M_\odot \text{ yr}^{-1}$ .

We note also that the results from the best fit agree with the empirical classification as “old passive” galaxy based on near-IR colours (see paper I).

As a cautionary note, we remind the reader that this object has been found variable over  $\sim 1$  month in the ISAAC photometry taken in the *SZ* band (see Richard et al. 2006). The *SZ* flux adopted here corresponds to the average between the 2 periods. It is currently unclear if and to which extent the apparent variability influences the results derived here.

## 5.3. A1835 - #17

This object is one of the few for which there is no ambiguity on the photometric redshift. See  $\chi^2$  map on Fig.9. This is mostly due to the fact that the stellar  $1.6 \mu\text{m}$  peak is clearly observed between the Ks band and the first two IRAC channels ( $3.6$  and  $4.5 \mu\text{m}$ ). With nearly all templates one obtains  $z_{\text{fit}} \sim 0.8$ ; a somewhat lower value of  $z_{\text{fit}} \sim 0.69$  is obtained with templates from the S04gyr group.

In all cases a very high extinction ( $A_V \sim 3-4$ ) is needed. However, models with very different ages yield fits of similar quality ( $\chi^2$ ): 7.5 Gyr with the BC models, 1 Gyr with Maraston models, and 10 Myr with the S04 templates. The SF histories correspond to bursts in all of them. This age uncertainty is most likely due to the fact that we rely here on the predictions in the rest-frame spectral range  $\sim 1.6-2.8 \mu\text{m}$ , where the evolutionary synthesis models are more uncertain than at shorter wavelengths. The stellar masses derived from the burst model fits are  $\sim (0.6 - 2.) \times 10^{10} / \mu M_\odot$  for the Maraston and BC templates and significantly smaller from the (younger) S04 template ( $M_\star \sim 7. \times 10^7 / \mu M_\odot$ ). For a value  $L_K/M = 3.2$  adopted for SCUBA galaxies (cf. Borys et al. 2005) one obtains  $M_\star = 3.1 \times 10^9 M_\odot$ , much lower than the typical masses of SCUBA galaxies. The magnification factor for this object is  $\mu \sim 1.2$  (cf. Table 4).

Using the semi-empirical GRASIL template group the best fits are found at  $z_{\text{fit}} = 0.78$  with the SED of the Sbc galaxy M 51 with an additional optical extinction of  $A_V \sim 3.8$ . The corresponding mid-IR to sub-mm SED is shown in Fig. 10, with a bolometric luminosity of  $5.5 \times 10^9 / \mu L_\odot$  corresponding to  $SFR = 0.9 / \mu M_\odot \text{ yr}^{-1}$ . If this object is indeed a very dusty starburst, which can in principle be verified with longer wavelength observations, it is much fainter than SCUBA galaxies (SMG) at the same redshift — e.g.  $\sim 4$  mag fainter in K (cf. Smail et al. 2004).

## 5.4. AC114-#1

Using the templates from synthesis models the best fits for this object are found between  $z_{\text{fit}} \sim 1$  and 2.5, with a secondary though less likely solution at high redshift (see Fig. 11). Over the interval  $\sim 1-2.5$  the photometric redshift is actually not well determined, since the curvature of the SED measured in the 4 IRAC bands is small and hence the position of the  $1.6 \mu\text{m}$  peak — the main constraint on  $z$  — only loosely constrained.

Both the BC and the Maraston templates give quite similar best fits:  $z_{\text{fit}} = 1.3-1.5$ , a burst with a maximal age of  $\sim 3.5-4.5$  Gyr, a stellar mass of  $\sim (1.6 - 2.6) \times 10^{12} / \mu M_\odot$  and a large extinction ( $A_V \sim 1.6-2.4$ ). The magnification factor for this object is  $\mu \sim 2.2$ . Best fits with a similar  $\chi^2$  are found using the S04gyr templates at  $z_{\text{fit}} = 1.6$  for a burst of 0.9–1.0 Gyr age with  $A_V = 2.8$  and a stellar mass corresponding to  $\sim 1.3 \times 10^{12} / \mu M_\odot$ .<sup>2</sup> The main difference between these models is a lower age and higher extinction in the latter.

<sup>2</sup> A lower mass  $M_\star = 2.4 \times 10^{11} / \mu M_\odot$  is obtained using Eq. 1 and  $L_K/M = 3.2$ .

Using the semi-empirical GRASIL templates yields a best fit at  $z_{\text{fit}} = 0.9\text{--}1.0$  for the M51 template. A strong additional extinction of  $A_V = 3.8$  is required, and the overall fit is lower quality (higher  $\chi^2$ ) than the fits discussed above. The overall SED resulting from these different fits is shown in Fig. 12. Interestingly the GRASIL template also reproduces quite well the observed MIPS  $24\ \mu\text{m}$  flux, although this was not included in the fit procedure. In any case the  $24\ \mu\text{m}$  flux is a strong indication for the presence of dust in this galaxy. In other words solutions with non negligible extinction at  $z \sim 0.9\text{--}1.5$  are favoured by this additional constraint.

If at  $z = 0.97$  the GRASIL template shown in Fig. 12 has a bolometric luminosity of  $2.8 \times 10^{11} / \mu L_\odot$  (close to the LIRG range) corresponding to  $\text{SFR} = 48 / \mu M_\odot$ , with  $\mu \sim 2$  (Table 4).

From the GRASIL SED shown here we may also expect a fairly strong sub-mm flux, in the range detectable with current instrumentation. To the best of our knowledge the southern cluster AC114 has so far not been observed in this spectral range.

### 5.5. Other EROs in A1835 – galaxies without Spitzer photometry

The objects treated here are those from Table 6 for which contamination by neighbouring sources does not allow us to determine photometry from the Spitzer images, i.e. the objects #3, #10, and #11 in Abell 1835. The main properties estimated for #3 and #10 are summarised in Table 6.

The SED of #11, shown in Fig. 1, precludes any reliable photometric redshift estimate; above  $z \gtrsim 1$  good fits can be found at all redshifts. For this reason this object is not discussed further.

As for other objects discussed earlier, #3 and #10 show a degeneracy between low and high- $z$ , with  $\chi^2$  minima found at  $z_{\text{fit}} \sim 1\text{--}1.5$  and  $5\text{--}6.0$  for #10 ( $5\text{--}6.5$  for #3). However, if at high- $z$  their absolute  $K_s$  restframe magnitude is of the order of  $-27.3$  to  $-27.6$ . Such high luminosity objects should be extremely rare; for this reason we subsequently only consider solutions with photometric redshifts below 4 and list the properties estimated from the best fit models.

**A1835-#3:** The best fit is obtained with the BC templates at  $z_{\text{fit}} = 1.12$  for a burst of 0.5 Gyr with an extinction of  $A_V = 0.8$ . The corresponding stellar mass is  $M_\star \sim 5.1 \times 10^9 / \mu M_\odot$ . Fits with the Maraston templates yield very similar parameters. A very similar mass ( $5.0 \times 10^9 / \mu M_\odot$ ) is also obtained using Eq. 1 and  $L_K/M = 3.2$  adopted for SCUBA galaxies (Borys et al. 2005).

**A1835-#10:** The best fit is obtained with the BC templates at  $z_{\text{fit}} = 1.23$  for a burst of 0.5 Gyr with an extinction of  $A_V = 1.8$ . The corresponding stellar mass is  $M_\star \sim 9.5 \times 10^9 / \mu M_\odot$ , basically identical to the one derived following Borys et al.. Fits with the Maraston templates yield a somewhat younger age (0.25 Gyr), lower extinction ( $A_V = 0.4$ ), and lower mass ( $6.4 \times 10^9 / \mu M_\odot$ ) at  $z_{\text{fit}} = 1.14$ .

To illustrate the expected IR to sub-mm SED of these objects we show, in Fig. 13, the best fits for #3 and #10 obtained with the GRASIL templates. For reference the best fit redshifts

obtained with the GRASIL templates are  $z_{\text{fit}} = 0.935$  and  $1.165$  for #3 and #10 respectively, and the SFR is  $\sim 2.4$  and  $4.3 M_\odot \text{ yr}^{-1}$ , assuming  $\mu = 1.4$  for both sources. The global SED and IR to sub-mm fluxes of these objects are quite similar to those of #17. Remember, however, that the sources #3 and #10 are blended with neighbouring object in the Spitzer images, hence requiring high spatial resolution observations to potentially resolve them with future instruments.

### 5.6. The importance of IRAC/Spitzer photometry on the photometric redshifts

For the objects with measurable IRAC photometry we have also examined the importance of this additional information on the SED fits and the resulting photometric redshifts. Overall this exercise, summarised in Fig. 14, shows that the objects can be grouped in three “classes”:

1) Objects showing degenerate/ambiguous low- and high- $z$  solutions even with IRAC photometry (cf. Fig. 3 with A1835-#2 shown in the top panel, also: A1835-#1 to some extend). For A1835-#2, formally the best fit is found in both cases (i.e. with or without IRAC photometry) at  $z \sim 7\text{--}7.5$ ). However, the solution at lower  $z$  is clearly favoured from arguments on the absolute magnitude of this object (cf. Sect. 4).

2) Degenerate/ambiguous low- and high- $z$  solutions whose degeneracy is lifted thanks to IRAC photometry (see A1835-#4, middle panel, and also AC114-#1). In this case the “curvature” measured between near-IR and the IRAC photometry allows one very clearly to locate the  $1.6\ \mu\text{m}$  stellar bump due to the minimum in the  $\text{H}^-$  opacity and hence to constrain the galaxy redshift. A1835-#1 is intermediate between this case and the following one (3).

3) Unconstrained photometric  $z$  from ground-based photometry, which becomes well defined low- $z$  solution with IRAC photometry (A1835-#17, bottom panel). This object, the faintest of our EROs in  $H$  and  $K_s$ , is a  $J$ -dropout. Therefore relying only on two ground-based near-IR photometric points results in a basically unconstrained photometric  $z$ , as shown in Fig. 14 (left bottom panel, dashed line). The two IRAC detections at  $3.6$  and  $4.5\ \mu\text{m}$  together with the upper limits at longer wavelength, are again attributed to the stellar  $1.6\ \mu\text{m}$  bump, making this object a very clear  $z \sim 0.81$  galaxy.

In conclusion, if sufficient near-IR ground-based and IRAC/Spitzer photometric datapoints can be secured and if they reveal a strong enough “curvature” such as to constrain the redshifted stellar  $1.6\ \mu\text{m}$  bump, SED fitting of EROs can yield fairly well defined photometric redshifts. In other cases, ambiguities between low- and high- $z$  may remain, and other arguments/data are needed to securely determine their redshift. However, given the resulting bright absolute magnitudes of these objects – if at high- $z$  – and their large number we consider the “low- $z$ ” ( $0 \lesssim z \lesssim 3$ ) solution much more likely for all of the objects studied here.

Although not included in the SED fitting procedure done with *Hyperz*, a measurement or a stringent upper limit of the  $24\ \mu\text{m}$  flux with MIPS can also provide important constraints, helping e.g. to distinguish between SED fits with or without



strong redenning and therefore indirectly to rule out certain redshifts (see e.g. the cases of A1835-#2, AC114-#1).

## 6. SED fitting of related objects

### 6.1. HUDF-J2 revisited

Using the same modeling technique and spectral templates described above, we have examined the optical ( $z_{850LP}$ ) drop-out object HUDF-J2 discussed by Mobasher et al. (2005) and more recently by Dunlop et al. (2006). This object was also selected by Yan et al. (2004) on the basis of its red  $3.6\ \mu\text{m}/z_{850LP}$ -band flux. Their full sample, named “IRAC” EROs (IEROs), will be discussed below (Sect. 6.2).

#### 6.1.1. Available photometry

Here we have used two datasets published for this object. (i): JHK photometry from NICMOS and ISAAC, IRAC/Spitzer data (channel 1–4), and the  $z_{850LP}$  non-detection from Mobasher et al. (2005). In addition the  $24\ \mu\text{m}$  flux measured by Mobasher et al. (2005) is also used for comparison, though not included in the *Hyperz* spectral fitting. (ii): same data as (i), except for revised values of the optical data from Dunlop et al. (2006) yielding a  $B_{435}$  non-detection plus detections in  $V_{606}$ ,  $i_{775}$  and  $z_{850LP}$ . Where necessary, quoted non-detection limits have been transformed to  $1\sigma$  limits for a consistent treatment with the *Hyperz* photometric redshift code.

#### 6.1.2. Results

Using the photometric dataset (i) from Mobasher et al. (2005) we find quite similar results as these authors, i.e. a degeneracy between solutions at  $z \sim 2.5$  plus significant extinction and at  $z \sim 6\text{--}7.5$  with zero/little extinction, with the formal best fits lying at high- $z$ . This is illustrated by the  $\chi^2$  maps shown in Fig. 15. The main results for this object are summarised in Table 7.

Concerning the high- $z$  solutions we note the following. The best fit  $z_{\text{phot}}$  depends somewhat on the spectral templates used; indeed using BCCWW or s04gyr templates we obtain  $z_{\text{fit}} \sim 7.39$  ( $\chi^2 = 1.5$ ) or  $z_{\text{fit}} \sim 6.5$  ( $\chi^2 = 1.2$ ). In both cases the best fit is obtained with zero extinction. With the same templates groups the best fit “low- $z$ ” solutions are  $z_{\text{fit}}=2.59$  and  $A_V = 1.8$  ( $\chi^2=2.3$ ) for the BCCWW templates, and  $z_{\text{fit}}=2.42$  and  $A_V = 3.4$  ( $\chi^2=2.6$ ) for the s04gyr templates. Test calculations have shown, introducing a minimum error of  $\sim 0.1\text{--}0.15$  mag already modifies considerably the  $\chi^2$  map leading to less well constrained solutions. Given uncertainties in the determination of measurement errors and uncertainties in matching photometry from different instruments (mainly NICMOS, ISAAC, and Spitzer) such errorbars may be more realistic than the small errors quoted by Mobasher et al. (2005). A comparison of the photometry of this object published by Yan et al. (2004, their object # 2) and the measurements of Mobasher et al. (2005), showing differences exceeding several  $\sigma$  in various bands, is also illustrative for this purpose. Given the relatively small differences in the  $\chi^2$ , the resulting exceptionally bright magnitude of this object ( $M^{\text{rest}}(Ks) \sim -27.$ , cf. Table 7), and

using the same “spirit” as for our EROs, we would conservatively favour a “low- $z$ ” interpretation for HUDF-J2 on this basis. Quantitatively the main weakness of the low- $z$  fits is the slight excess predicted in the  $z_{850LP}$  band with respect to the photometry from Mobasher et al., as shown in Fig. 16. Actually the flux predicted with the BCCWW template (black line) corresponds to a  $2\sigma$  detection; a somewhat larger flux is predicted with the GRASIL templates.

Recently, Dunlop et al. (2006) have questioned the very deep  $z_{850LP}$  non-detection limit quoted by Mobasher et al. (2005), and they have performed manual photometry of HUDF-J2 in the optical bands. Their faint detection in  $V_{606}$ ,  $i_{775}$ , and  $z_{850LP}$  alters the balance of the  $\chi^2$  behaviour between low- $z$  and high- $z$  favouring solutions at  $z_{\text{fit}} = 2.15 \pm 0.3$  (Dunlop et al. 2006). However, imposing a measurement in a prescribed aperture may not be appropriate. If we use the same constraint and the BC templates we obtain  $z_{\text{fit}} = 2.48$ ,  $A_V = 3.0$ , and a burst of 0.26 Gyr age, in good agreement with Dunlop et al. (2006). In any case, the model fluxes shown in Fig. 16 in the  $z_{850LP}$  band and at shorter wavelengths, are nicely bracketed by the measurements of Dunlop et al. and Mobasher et al.

As qualitatively the SED of HUDF-J2 resembles that of our EROs (in particular that of A1835-#2), and given that “low- $z$ ” fits indicate significant extinction, it is instructive to explore also spectral templates of dusty objects. Indeed, using the GRASIL templates a reasonable fit ( $\chi^2=4.8$ ) to the observations (i) are found with the M82 template and additional extinction of  $A_V = 2.8$  at  $z_{\text{fit}} \sim 1.8$  (see red line in Fig. 17). Adopting the photometry from (ii), an excellent fit ( $\chi^2=0.9$ ) is found with the HR10 template and no additional extinction for  $z_{\text{fit}} = 2.31$  (blue line in Fig. 17). Interestingly, both fits reproduce quite well the  $24\ \mu\text{m}$  flux observed by MIPS/Spitzer (Mobasher et al. 2005), which was not included in our fit procedure. This lends further credit to the explanation of HUDF-J2 as a dust rich galaxy at  $z \sim 2.3$ . For comparison, Mobasher et al. do not fit the  $24\ \mu\text{m}$  emission, and invoke other components – possibly an obscured AGN – to explain this flux. And this measurement is not considered by Dunlop et al. (2006) in their analysis. As also shown by Fig. 17, the predicted far-IR to sub-mm flux of HUDF-J2 should be within reach of existing/future facilities. Detections in this spectral range should definitely be able to distinguish between dust-free high- $z$  solutions and the “low- $z$ ” fits favoured here.

From the two GRASIL fits shown in Fig. 17 with the M82 and HR10 templates at  $z_{\text{fit}} = 1.83$  and  $2.52$  respectively we estimate a bolometric luminosity of  $L_{\text{bol}} \sim (4.2\text{--}6.2) \times 10^{11} L_{\odot}$  (in the LIRG range) corresponding to  $\text{SFR} \sim 72\text{--}107 M_{\odot} \text{ yr}^{-1}$ .

### 6.2. IRAC selected EROs in the HUDF

To compare our objects with the IRAC selected EROs in the HUDF from Yan et al. (2004) discussed in paper I, we have subjected them to the same quantitative analysis using *Hyperz*. The results from the SED fits are summarised in Table 8. Note that for simplicity we list fit results using Bruzual & Charlot templates only, although computations were also carried out using the other template groups. Furthermore, to account for

possible mismatches between the photometry from different instruments (ACS, NICMOS, ISAAC, and IRAC) and to allow for other uncertainties in the error quantification, we adopt a minimum error of 0.1 mag in all filters.

### 6.2.1. Properties of IRAC EROs

As already noted by Yan et al., four objects have quite uncertain photometric redshifts. #1, 2, and 10 have quite degenerate  $\chi^2$  over a large redshift range. #5 yields the worst fit, due to an apparent flux excess at  $8 \mu\text{m}$ , which could be an indication for an AGN contribution. Therefore we follow Yan et al. and exclude these objects from the subsequent discussion of the average properties of this sample. However, it is worth mentioning that #2 corresponds to the HUDF-J2 object from Mobasher et al. (2005) discussed above.

The main difference with the results of Yan et al. is that, once allowing for a reasonable minimum error of say 0.1 mag and including a wide variety of star formation histories and varying extinction, we are able to obtain good fits to all objects (except those already mentioned) with standard Bruzual & Charlot templates, i.e. there is no need for composite stellar populations as invoked by Yan et al. (2004). In consequence, our best fit ages and extinction differ systematically from their analysis, as will be discussed below. Otherwise quite similar properties are derived from our more complete quantitative analysis.

More precisely we find best fit redshifts ranging from 0.6 to 2.8 with a median (mean) of 1.6 (1.9). The redshifts difference with Yan et al. has a median value of  $\delta z/(1+z) \approx -0.07$ . In particular we obtain significantly lower redshifts for two objects, #13 and 14. However their photometric redshifts turn out to be quite uncertain and strongly dependent on the template set used<sup>3</sup>. We therefore consider them as quite insecure. Spectroscopic redshifts are available for 3 sources of the Yan et al. sample, #9, #13, and #17 (see Daddi et al. 2005 and update by Maraston et al. 2006). Except for the uncertain object #13 just discussed, the agreement with our photometric redshifts is excellent ( $|\delta z| \leq 0.05$ ).

If taken at face value our best fits yield the following average properties for these IRAC selected EROs (cf. Table 8): a median (average) extinction of  $A_V = 2.0$  (2.2), a median (average) age of 0.5 (1.3) Gyr, and stellar masses  $M_\star$  ranging between  $10^9$  and  $5 \times 10^{11} M_\odot$ , with a median (average) mass of  $0.5 \times 10^{11}$  ( $1.3 \times 10^{11}$ )  $M_\odot$ <sup>4</sup>.

Their absolute  $M_{AB}^{\text{rest}}(K_s)$  covers -20.5 to -24.3 in AB mags, with a median of -22.3, corresponding to a median of  $M_{\text{Vega}}^{\text{rest}}(K_s) = -24.2$ . This is somewhat brighter than  $M^\star$  from 2MASS (-23.53 cf. Kochanek et al. 2001) but similar to  $M^\star$  at  $z \sim 0.6$ –2.5 from Bolzonella et al. (2002) and Kashikawa et al. (2003) who find  $M_{\text{Vega}}^\star(K_s) \sim -24.3$  to -25.0.

As already mentioned these average properties are in good agreement with those derived by Yan et al. (2004), except that

we find good fits with templates computed assuming standard star formation histories, i.e. that we do not need to invoke other more arbitrary composite stellar populations. In consequence, the bulk of the fits we obtain correspond to younger stellar ages and hence to higher extinction than Yan et al.. As already mentioned by these authors, observations at longer wavelengths (including MIPS imaging) could help to distinguish between these solutions; in fact, according to Yan (2006, private communication) 9 of the 17 IERO have been detected at  $24 \mu\text{m}$  with fluxes above  $20 \mu\text{Jy}$  providing support to our interpretation.

For the subsequent comparison we adopt the properties derived here as representative values for the IRAC selected EROs.

### 6.2.2. Comparison with our ERO sample

Empirically our optical drop-out EROs share many properties with the IRAC selected EROs (cf. paper I), in particular similar optical to near-IR and IRAC/Spitzer colours, and similar  $z_{850\text{LP}}$ , near-IR and IRAC/Spitzer magnitudes, after correcting for our median magnification factor corresponding to  $\sim 0.4$  mag. In contrast to our EROs, which so far are undetected in all bands shortward of  $z_{850\text{LP}}$ , the IRAC selected EROs of Yan et al. (2004) are detected in optical bands (BVIZ), although at very faint magnitudes (e.g.  $V \sim 27$  to 30.). As the depth of this data, taken from the Hubble Ultra Deep Field, is deeper than our optical photometry, this is not incompatible with the two samples being very similar.

The similarity between our EROs and the IRAC selected EROs of Yan et al. (2004) is also evident from the comparison of the derived properties (cf. Tables 5 and 8), showing similar redshifts, extinction, stellar ages, and stellar masses.

## 7. Discussion

A fact worth mentioning concerning the objects discussed here is that one of the sources, AC114-#1, fulfills the criteria commonly used to select  $z \sim 6$  galaxies as *i*-dropout. Indeed for this object  $(I_{814} - z_{850\text{LP}})_{AB} > 2.16$  and it is undetected at all wavelengths shorter than  $z_{850\text{LP}}$ . Thus the commonly adopted *i* dropout criterion for ACS observations,  $(I_{775W} - z_{850\text{LP}})_{AB} > 1.5$  (cf. Stanway et al. 2003, Dickinson et al. 2004) yielding  $(I_{775W} - z_{850\text{LP}})_{AB} > 1.85$  once transformed to the  $I_{814}$  filter from WFPC2 (Sirianni et al. 2005), is satisfied by this ERO. Furthermore, the flux expected in B and V filters from our SED fits is sufficiently low ( $V_{F606W} \gtrsim 29.2$  in AB mag) that it would remain undetected in the GOODS imaging with ACS (cf. Giavalisco et al. 2004). Therefore such a low redshift object, with an intrinsic lensing corrected magnitude of  $z_{850\text{LPAB}} \sim 26.$ , could potentially contaminate *i*-dropout samples. Apparently this is not the case for the sample of IRAC selected EROs from Yan et al. (2004), which if detected in  $z_{850\text{LP}}$  are also detected at shorter wavelengths.

Obviously, observations in several filters longward of  $z_{850\text{LP}}$  are able to eliminate such objects with very red SEDs out to the IR. For example, examining  $J - H$  Stanway et al. (2005) find that their  $i_{775W}$ -dropout sample is consistent with unreddened high- $z$  starbursts. On the other hand, in a recent analysis combining ACS and Spitzer imaging of the GOODS field, Yan

<sup>3</sup> Using the s04gyr (Maraston) templates we find best fits at  $z_{\text{fit}} = 2.3$  (2.1) and (0.7) 1.3 for #13 and 14 respectively.

<sup>4</sup> Note that our models assume a Miller-Scalo IMF from 0.1 to 125  $M_\odot$ , whereas Yan et al. (2004) adopt a Chabrier (2003) IMF.

**Table 5.** Derived/estimated properties for optical dropout ERO galaxies with near-IR and Spitzer detections. Listed are the object ID (col. 1), the photometric redshift estimate (col. 2), the extinction (col. 3), the type of the best fit template (col. 4), the distance modulus corresponding to  $z_{\text{phot}}$  (col. 5), the absolute  $Ks$ -band magnitude non-corrected for lensing (col. 6), the absolute rest-frame  $Ks$ -band magnitude non-corrected for lensing (col. 7), the estimated stellar mass (from scaling the SED fit or from  $M^{\text{rest}}(Ks)$  assuming  $L_K/M = 3.2$ , col. 8), the estimated star formation rate non-corrected for lensing (col. 9), and the age of the stellar population (col. 10). To correct the above mentioned absolute quantities for gravitational magnification the appropriate magnification factors listed in Table 4 must be used.

| Object    | $z_{\text{phot}}$ | $A_v$<br>[mag] | template                  | DM <sup>a</sup><br>[mag] | $M^{\text{rest}}(Ks) - 2.5 \log(\mu)$<br>[mag] | Mass $\times\mu$<br>$M_\odot$ | SFR $\times\mu$<br>$M_\odot \text{ yr}^{-1}$ | stellar age<br>[Gyr] |
|-----------|-------------------|----------------|---------------------------|--------------------------|--|-------------------------------|--|----------------------|
| A1835-#1  | $\sim 0.4-1.5$    | ?              | Fits uncertain – see text |                          |  |                               |  |                      |
| A1835-#2  | $\sim 2.8-3$      | 2.4–3          | young burst               | 47.0                     | -27.7  | $\sim 1.2 \times 10^{12}$     | $\sim 2100$                                  | $< 0.36$             |
| A1835-#4  | $\sim 1.2$        | 0–1.6          | burst/elliptical          | 44.60                    | -21.6  | $\sim 1.7 \times 10^{10}$     | $\sim 5$                                     | 0.7 to 4.5           |
| A1835-#17 | $\sim 0.7-0.8$    | $\sim 3.8$     | burst                     | 43.0                     | -21.7  | $\sim 1.3 \times 10^{10?}$    | $\sim 0.9$                                   | ? (see text)         |
| AC114-#1  | $\sim 1.3-1.6$    | $\sim 1.6-2.8$ | burst                     | 44.84                    | -26.4  | $(1.3 - 2.6) \times 10^{12}$  |  | $\sim 0.9-4.5$ Gyr   |
| AC114-#1  | $\sim 1.0$        | +3.8           | M51                       | 44.03                    | -25.9  |                               | $\sim 48$                                    |                      |

<sup>a</sup> distance modulus computed for minimum redshift

**Table 6.** Same as Table 5 for optical dropout ERO galaxies detected only in the near-IR (no Spitzer photometry available). No information is listed for A1835-#11 due to its highly uncertain photometric redshift.

| Object    | $z_{\text{phot}}$ | $A_v$<br>[mag] | template | DM<br>[mag] | $M^{\text{rest}}(Ks) - 2.5 \log(\mu)$<br>[mag] | Mass $\times\mu$<br>$M_\odot$ | SFR $\times\mu$<br>$M_\odot \text{ yr}^{-1}$ | stellar age<br>[Gyr] |
|-----------|-------------------|----------------|----------|-------------|--|-------------------------------|--|----------------------|
| A1835-#3  | $\sim 1.1$        | $\sim 0.6-0.8$ | burst    | 44.4        | -22.2  | $\sim 5.1 \times 10^9$        |  | 0.5                  |
| A1835-#10 | $\sim 1.2$        | $\sim 1.8$     | burst    | 44.68       | -22.9  | $\sim 9.5 \times 10^9$        |  | 0.5                  |
| A1835-#11 | ?                 |                |          |             |  |                               |  |                      |

**Table 7.** Same as Table 5 for the HUDF-J2 galaxy from Mobasher et al. (2005). To the best of our knowledge no lensing correction has to be applied to this object ( $\mu = 1$ ).

| Object  | $z_{\text{phot}}$ | $A_v$<br>[mag] | template | DM <sup>a</sup><br>[mag] | $M^{\text{rest}}(Ks)$<br>[mag] | Mass<br>$M_\odot$          | SFR<br>$M_\odot \text{ yr}^{-1}$ | stellar age<br>[Gyr] |
|---------|-------------------|----------------|----------|--------------------------|--------------------------------|----------------------------|----------------------------------|----------------------|
| HUDF-J2 | $\sim 2.4-2.6$    | $\sim 1.8-3.4$ | burst    | $\sim 46.47$             | -24.1 to -24.5                 | $\sim 5. \times 10^{11}$   |                                  | $\lesssim 0.6-2.$    |
| HUDF-J2 | $\sim 6.4-7.4$    | $\sim 0$       | burst    | 49.03                    | -26.9                          | $(2. - 3.) \times 10^{12}$ |                                  | $\lesssim 0.7$       |
| HUDF-J2 | $\sim 2.5$        |                | HR10     | 46.58                    | -23.9                          |                            | 107                              |                      |
| HUDF-J2 | $\sim 1.8$        | $\sim +2.8$    | M82      | 45.73                    | -23.0                          |                            | 72                               |                      |

et al. (2006) find that  $\sim 15-21$  % of the IRAC detected  $i_{775W}$ -dropouts have very high flux ratios between  $3.6 \mu\text{m}$  and the  $z_{850LP}$  band. These amount to  $\sim 4$  % of their total  $i$  dropout, i.e.  $z \approx 6$  sample. Our object, AC114-#1, belongs very likely to the same class of rare objects.

## 8. Conclusions

We have undertaken a detailed analysis of the stellar populations and the extinction of a sample of 8 lensed EROs in Abell 1835 and AC114 from Richard et al. (2006) and related objects from the Hubble Ultra Deep Field (HUDF). The analysis includes in particular one known SCUBA galaxy (SMMJ14009+0252), the  $z \sim 6.5$  post-starburst galaxy candidate from Mobasher et al. (2005), and the IRAC selected EROs from Yan et al. (2004).

Empirically, these objects share a very red overall SED, similar colours and magnitudes, and very faint or absent flux in optical bands. In particular most of our EROs, originally selected as very red ( $R - Ks > 5.6$ ) optical drop-out objects by

Richard et al., have been detected with ACS/HST in deep  $z_{850LP}$  images, as discussed in Hempel et al. (2006, paper I).

The ACS, VLT, and IRAC/Spitzer photometry has been taken from paper I. To determine photometric redshifts and to simultaneously constrain the stellar population and extinction properties of these objects, we have used an updated version of the *Hyperz* code from Bolzonella et al. (2000) including a large number of synthetic, semi-empirical and empirical spectral templates.

The main results from the SED fitting are the following:

- The SED analysis including near-IR plus IRAC photometry for 5 of our objects, shows in most cases degenerate solutions between “low- $z$ ” ( $z \sim 1-3$ ) and high- $z$  ( $z \sim 6-7$ ) for their photometric redshifts. Although formally best fits are often found at high- $z$ , their resulting bright absolute magnitudes, the number density of these objects, and in some cases Spitzer photometry or longer wavelength observations, strongly suggest that all of these objects are at “low- $z$ ”.

**Table 8.** Derived/estimated properties for IRAC selected EROs from Yan et al. (2004) from *Hyperz* fits with Bruzual & Charlot templates with different star formation histories, and computed assuming a minimum error of 0.1 mag in all bands. Note: all magnitudes are in the Vega system ( $M(Ks)_{\text{Vega}} = M(Ks)_{\text{AB}} - 1.871$ ).

| Object          | $z_{\text{Yan}}$ | $z_{\text{phot}}$ | template       | age<br>[Gyr] | $A_v$<br>[mag] | DM<br>[mag] | $M^{\text{rest}}(Ks)$<br>[mag] | Mass<br>$M_{\odot}$ |
|-----------------|------------------|-------------------|----------------|--------------|----------------|-------------|--------------------------------|---------------------|
| 1*              | 3.6              | 2.5               | burst          | 0.7          | 2.4            | 46.60       | -25.85                         | 3.4e+11             |
| 2*a             | 3.4              | 2.1               | burst          | 0.7          | 2.8            | 46.12       | -25.06                         | 1.7e+11             |
| 3               | 2.9              | 2.8               | $\tau = 1$ Gyr | 2.6          | 2.0            | 46.82       | -25.9                          | 3.5e+11             |
| 4               | 2.7              | 1.6               | $\tau = 1$ Gyr | 4.5          | 2.0            | 45.43       | -24.02                         | 7.7e+10             |
| 5*              | 2.8              | 3.0               | $\tau = 1$ Gyr | 2.3          | 2.2            | 47.04       | -26.22                         | 2.1e+11             |
| 6               | 2.3              | 1.1               | burst          | 0.01         | 3.8            | 44.40       | -22.8                          | 1.2e+09             |
| 7               | 2.7              | 2.6               | $\tau = 5$ Gyr | 2.6          | 1.8            | 46.69       | -25.66                         | 5.2e+11             |
| 8               | 2.9              | 2.7               | $\tau = 1$ Gyr | 2.3          | 1.4            | 46.71       | -26.13                         | 3.8e+11             |
| 9               | 2.8              | 2.7               | burst          | 0.4          | 1.0            | 46.76       | -25.19                         | 1.4e+11             |
| 10*             | 2.1              | 0.9               | burst          | 0.2          | 3.8            | 43.75       | -20.58                         | 8.3e+08             |
| 11              | 2.4              | 1.6               | burst          | 0.006        | 3.8            | 45.36       | -23.4                          | 6.2e+09             |
| 12              | 1.9              | 2.5               | burst          | 0.4          | 0.6            | 46.55       | -23.54                         | 2.9e+10             |
| 13 <sup>b</sup> | 1.9              | 0.7               | burst          | 0.2          | 3.8            | 43.00       | -22.38                         | 9.5e+08             |
| 14 <sup>b</sup> | 1.6              | 0.6               | $\tau = 5$ Gyr | 2.6          | 3.8            | 42.61       | -22.79                         | 2.1e+10             |
| 15              | 2.7              | 2.7               | $\tau = 1$ Gyr | 1.7          | 1.0            | 46.75       | -24.16                         | 5.2e+10             |
| 16              | 2.4              | 1.6               | burst          | 0.01         | 2.4            | 45.44       | -24.33                         | 5.0e+09             |
| 17              | 1.6              | 1.7               | burst          | 0.5          | 0.8            | 45.50       | -24.38                         | 5.1e+10             |

\* Uncertain photometric redshifts

<sup>a</sup> same as object HUDF-J2 from Mobasher et al. (2005)

<sup>b</sup>  $z_{\text{phot}}$  redshift likely underestimated (see text)

- The majority of our lensed objects are best understood by relatively young ( $\lesssim 0.5$ – $0.7$  Gyr) and dusty starbursts.
- For 3 of our objects we find indications for strong extinction, with  $A_v \sim 2.4$ – $4$ . Among them, the galaxy SMMJ14009+0252 is a known sub-mm emitter and at least one of them, the ERO AC114-# 1, is predicted to be in the LIRG category and expected to be detectable with current sub-mm instruments. For the remaining objects, among which 3 show moderate to strong extinction, we present predictions of their IR to sub-mm SEDs for future observations with APEX, Herschel, and ALMA.
- The stellar masses estimated for our objects span a large range from  $\sim 5. \times 10^9 / \mu$  to  $1. \times 10^{12} / \mu M_{\odot}$ , where  $\mu$  is the magnification factor derived from the gravitational lensing model. Typically one has  $\mu \sim 1.2$ , with a maximum magnification of  $\lesssim 2$ . Where appropriate, star formation rates estimated from the bolometric luminosity determined from spectral template fitting are  $\text{SFR} \sim (1 - 36) / \mu M_{\odot} \text{ yr}^{-1}$ . For SMMJ14009+0252, the most extreme case, we estimate  $L_{\text{bol}} \sim 6. \times 10^{11} L_{\odot}$  and  $\text{SFR} \sim 1000 M_{\odot} \text{ yr}^{-1}$  for  $z_{\text{fit}} \sim 3$  and  $\mu = 2$ .
- Taking uncertainties and revisions of the photometry of HUDF-J2 as well as accounting for a variety of spectral templates, we suggest that this object, originally identified as a  $z \sim 6.5$  massive post-starburst, is more likely a dusty starburst at  $z \sim 2.3$ – $2.6$  in agreement with the reanalysis by Dunlop et al. (2006). We show that this explanation also naturally explains the observed  $24 \mu\text{m}$  emission from this object and we predict its IR to sub-mm SED.
- Using the same methods we have analysed the sample of IRAC selected EROs from Yan et al. (2004). Both empirically and from our SED fits we find that these objects show

very similar properties to our lensed EROs. In contrast to Yan et al. we do not find strong indications for composite stellar populations in these objects.

*Acknowledgements.* We’ve benefited from interesting discussions with numerous colleagues we’d like to thank here collectively. We thank Haojing Yan for private communication of MIPS data. Support from *ISSI* (International Space Science Institute) in Bern for an “International Team” is kindly acknowledged. This work was supported by the Swiss National Science Foundation, the French *Centre National de la Recherche Scientifique*, and the French *Programme National de Cosmologie* (PNC) and *Programme National de Galaxies* (PNG).

## References

- Alexander, D., et al. 2004, in “Multiwavelength Mapping of Galaxy Formation and Evolution”, Eds. R. Bender, A. Renzini, Springer Verlag [astro-ph/0401129]
- Alexander et al. 2005, *Nature*, 434, 738
- Alonso-Herrero, A., et al., 2004, *ApJS*, 154, 155
- Alonso-Herrero, A., et al., 2006, *ApJ*, 640, 167
- Aretxaga, I., et al., 2003, *MNRAS*, 342, 759
- Blain, A.W., et al., 2002, *Physics Report*, 369, 111
- Bolzonella, M., Miralles, J.-M., Pelló, R., 2000, *A&A*, 363, 476
- Bolzonella, M., Pelló, R., Maccagni, D., 2002, *A&A*, 395, 443
- Bouwens, R. J., Illingworth, G. D., Blakeslee, J. P., Franx, M., 2006, *ApJ*, 653, 53
- Borys, C., Smail, I., Chapman, S. C., Blain, A. W., Alexander, D. M., & Ivison, R. J. 2005, *ApJ*, 635, 853
- Bruzual, G., Charlot, S., 2003, *MNRAS*, 344, 1000

- Calzetti, D., Kinney, A.L., Storchi-Bergmann, T. 1994, *ApJ*, 429, 582
- Calzetti D., Armus L., Bohlin R. C., Kinney A. L., Koornneef J., Storchi-Bergmann T., 2000, *ApJ*, 533, 682
- Campusano, L.E., Pelló, R., Kneib, J.-P., Le Borgne, J.-F., Fort, B., Ellis, R., Mellier, Y., Smail, I., 2001, *A&A*, 378, 394
- Coleman, D.G., Wu, C.C., Weedman, D.W. 1980, *ApJS*, 43, 393
- Daddi, E., et al., *ApJ*, 626, 680
- Dannerbauer et al. 2002, *ApJ*, 573, 473
- Dickinson, M., et al. 2004, *ApJ*, 600, L99
- Dunlop, J.S., Cirasuolo, M., McLure, R.J., 2006, *MNRAS*, submitted [astro-ph/0606192]
- Egami, E., et al., 2004, *ApJS*, 154, 130
- Gavignaud, I., et al., 2006, *A&A*, 457, 79
- Giavalisco, M., et al., 2004, *ApJ*, 600, L93
- Frayser et al. 2004, *AJ*, 127, 728
- Hempel, A., et al., 2007, *A&A*, to be submitted (paper I)
- Hughes et al. 1998, *Nature*, 394, 241
- Iverson et al. 2000, *MNRAS*, 315, 209
- John, T.L., 1998, *A&A*, 193, 189
- Kashikawa et al., 2003, *AJ*, 125, 53
- Kennicutt, R.J., 1998, *ARAA*, 36, 182
- Kinney, A., Calzetti, D., Bohlin, R. C., McQuade, K., Storchi-Bergmann, T., & Schmitt, H. R., 1996, *ApJ*, 467, 38
- Kochanek et al. 2001, *ApJS*, 60, 566
- Koekemoer, A.M., et al., 2004, *ApJ*, 600, L123
- Leitherer, C., et al., 1999, *ApJS*, 123, 3
- Maraston, C., 2005, *MNRAS*, 362, 799
- Maraston, C., et al., 2006, *ApJ*, 652, 85
- McCarthy, P.J., 2004, *ARAA*, 42, 477
- Mobasher, B., et al., 2005, *ApJ*, 635, 832
- Natarajan, P., Kneib, J.-P., Smail, I., Ellis, R.S., 1998, *ApJ*, 499, 600
- Pelló, R., et al., 2004, *A&A*, 416, L35
- Richard, J., et al., 2006, *A&A*, 456, 861
- Rigby, J.R., et al., 2006, *ApJ*, 627, 134
- Rigopoulou, D., et al., 2006, *ApJ*, 648, 81
- Sawicki, M., 2002, *AJ*, 124, 3050
- Schaerer, D., 2002, *A&A*, 382, 28
- Schaerer, D., 2003, *A&A*, 397, 527
- Schaerer, D., Pelló, R., 2005, *MNRAS*, 362, 1054
- Schaerer, D., et al., 2006, *The Messenger*, 125, 20
- Silva, L., Granato, G. L., Bressan, A., & Danese, L. 1998, *ApJ*, 509, 103
- Smail et al. 2000, *ApJ*, 528, 612
- Sirianni, M., et al., 2005, *PASP*, 117, 1049
- Smail et al. 2002, *MNRAS*, 331, 495
- Smail et al. 2004, *ApJ*, 616, 71
- Smith, G. P., Kneib, J.-P., Smail, I., Mazzotta, P., Ebeling, H., & Czoske, O. 2005, *MNRAS*, 359, 417
- Stanway, E.R., Bunker, A.J., McMahon, R.G., 2003, *MNRAS*, 342, 439
- Stanway, E.R., McMahon, R.G., Bunker, A.J., 2003, *MNRAS*, 359, 1184
- Stern, D., 2006, *AJ*, 132, 1405
- Takata, T., et al. 2006, *ApJ*, in press [astro-ph/0607580]
- Veilleux, S., Kim, D.-C., Sanders, D.B., 1999, *ApJ*, 522, 113
- Yan, H., et al., 2003, *ApJ*, 585, L93
- Yan, H., et al., 2004, *ApJ*, 616, 63
- Yan, H., et al., 2006, *ApJ*, 651, 24
- Zheng W., Kriss G. A., Telfer R. C., Grimes J. P., Davidsen A. F., 1997, *ApJ*, 475, 469

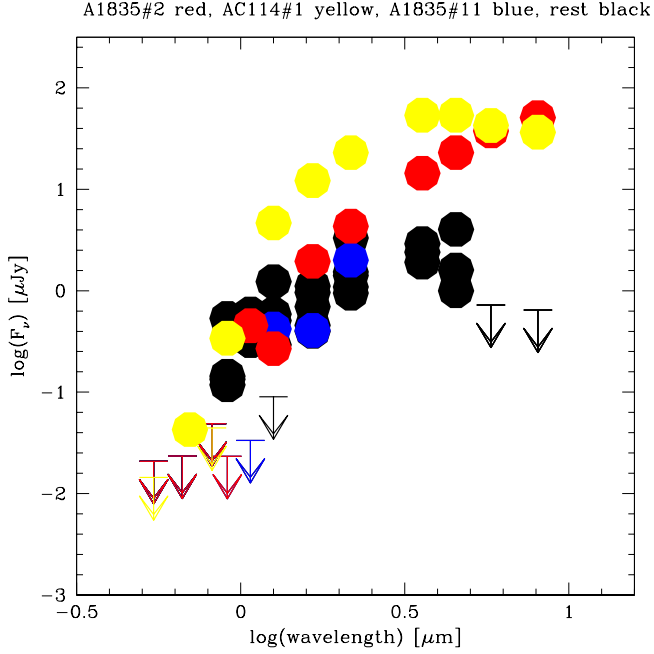


**Fig. 1.** Observed SED of all EROs in the optical and near-IR up to 10  $\mu\text{m}$ . The two most extreme objects, the sub-mm galaxy A1835-#2 and AC114-#1, are indicated in red and yellow respectively. A1835-#11, whose properties including the photometric redshift remain highly uncertain is shown in blue.

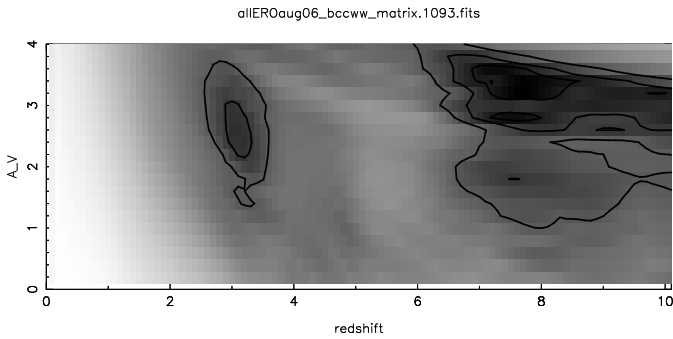


**Fig. 2.**  $\chi^2$  map as a function of redshift and extinction ( $\chi^2(z, A_V)$ ) for A1835-#2, displaying in dark the most probable regions on a logarithmic scale. Solid lines enclose the 1 to 3  $\sigma$  contours (confidence levels of 68, 90 and 99 % respectively). The  $(z, A_V)$  projection plane presented in this figure corresponds to the best  $\chi^2$  found through the model-age parameter space for templates from the BCCWW group. Note the degeneracy of the photometric redshift solutions in this plane. Formally the best fit is found at high redshift ( $z_{\text{fit}} > 7$ ). However, for various reasons, including the 24  $\mu\text{m}$  and sub-mm SED and the exceptional luminosity of this object if at high  $z$ , the most likely redshift of this galaxy is  $\sim 3$ . See discussion in text.

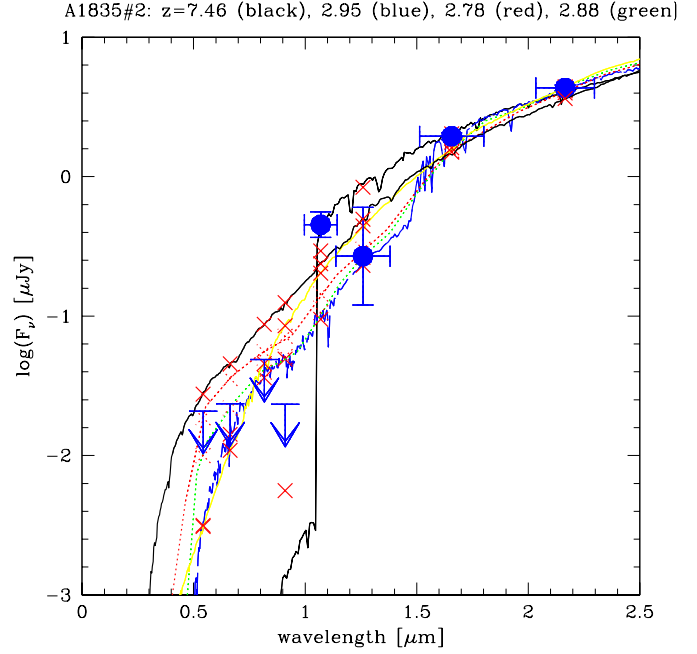


**Fig. 3.** A1835-#2: Comparison of best fit high- $z$  solution (black,  $z_{\text{fit}}=7.46$ ) with model fits at  $z \sim 3$ . Blue: Bruzual & Charlot model (SF history as ellipticals at age of 0.36 Gyr + 2.4 mag  $A_V$  extinction). Red: GRASIL template of NGC 6090 with  $A_V=1.4$ . See discussion in text.

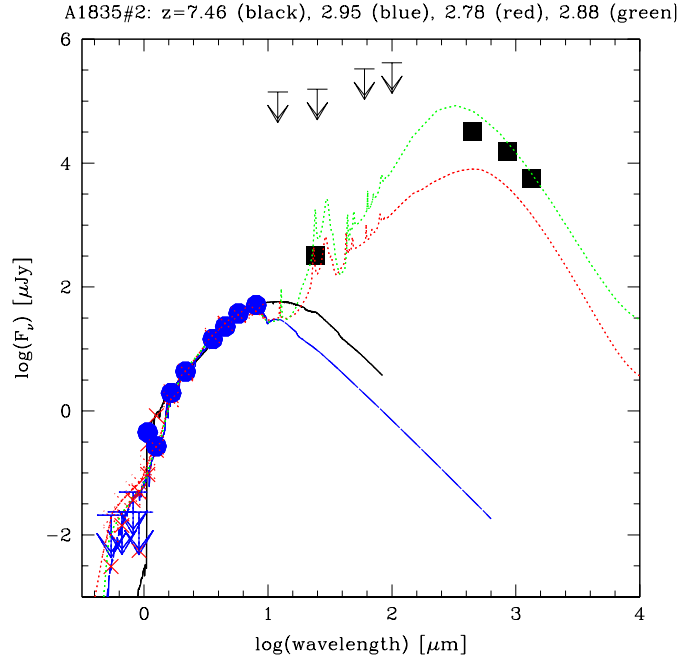


**Fig. 4.** Observed SED of the ERO/sub-mm galaxy A1835-#2 including VLT, Spitzer (IRAC, MIPS), SCUBA observations. The model fits are the same as shown in Fig. 3. Note that the two fits with GRASIL models at  $z \sim 2.8$ – $2.9$  reproduce well the MIPS 24  $\mu\text{m}$  flux and bracket the observed sub-mm points.

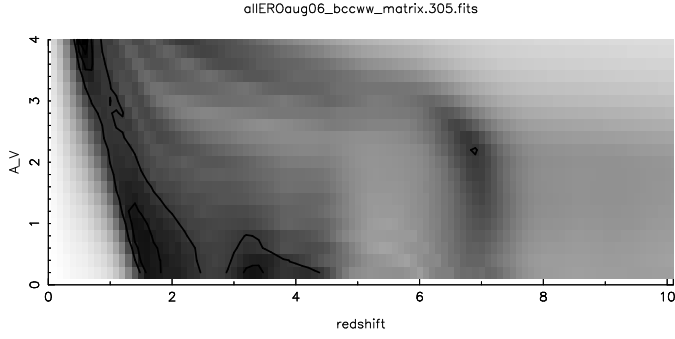


**Fig. 5.** Same as Fig. 2 for A1835-#1.

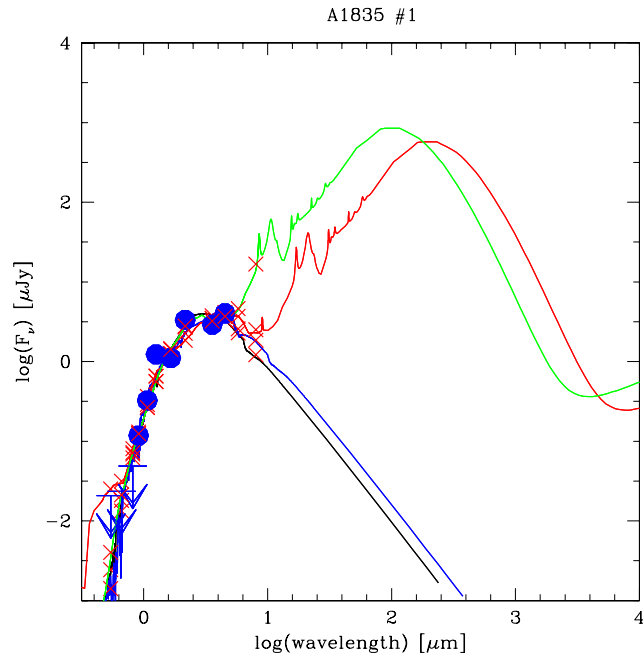


**Fig. 6.** A1835-#1: Comparison between fits with Bruzual and Charlot models at  $z = 0.50$  (black) and  $1.35$  (blue), and fits with dusty starburst models from GRASIL templates at  $z = 1.75$  (M82, red) and  $0.4$  (green, M82 plus additional extinction of  $A_V = 3.8$ ).

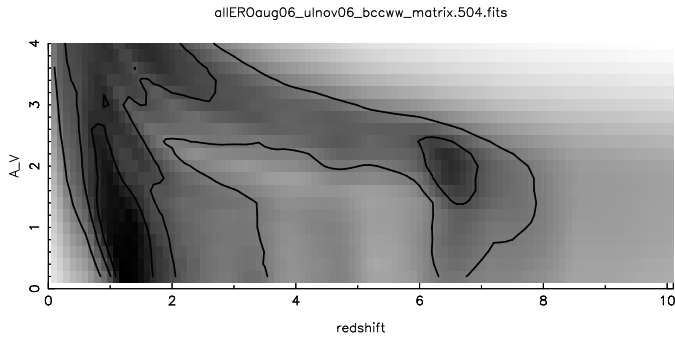


**Fig. 7.** Same as Fig. 2 for A1835-#4.

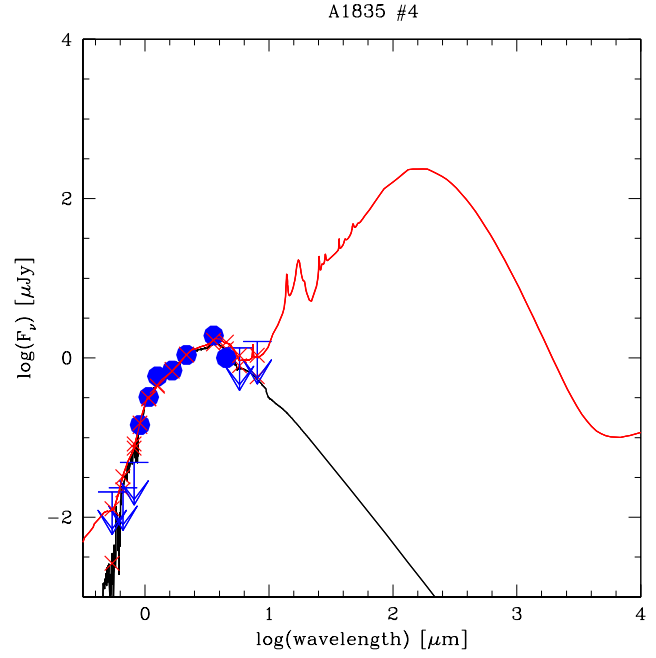


**Fig. 8.** A1835-#4: Comparison between fits with BCCWW galaxy template at  $z = 1.20$ , and fits with the M82 template from GRASIL at  $z = 1.24$  (and no additional extinction).

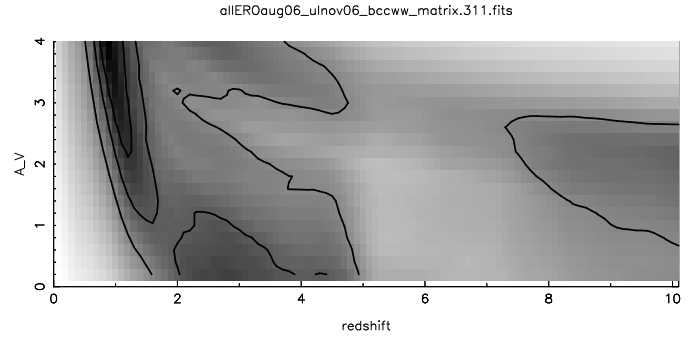


**Fig. 9.** Same as Fig. 2 for A1835-#17.

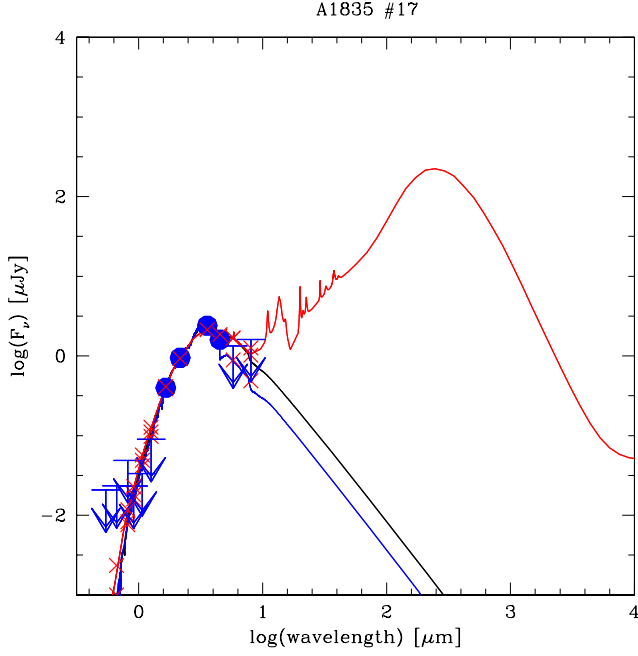


**Fig. 10.** A1835-#17: Comparison between fits with Maraston (2005) templates at  $z = 0.81$  and  $A_V = 1.$ , and fits with dusty starburst models from GRASIL templates at  $z = 0.60$  and  $0.79$  plus additional extinction of  $A_V \sim 3.6$ . Note that the Maraston template does not include dust emission, which would be expected for such high an extinction.

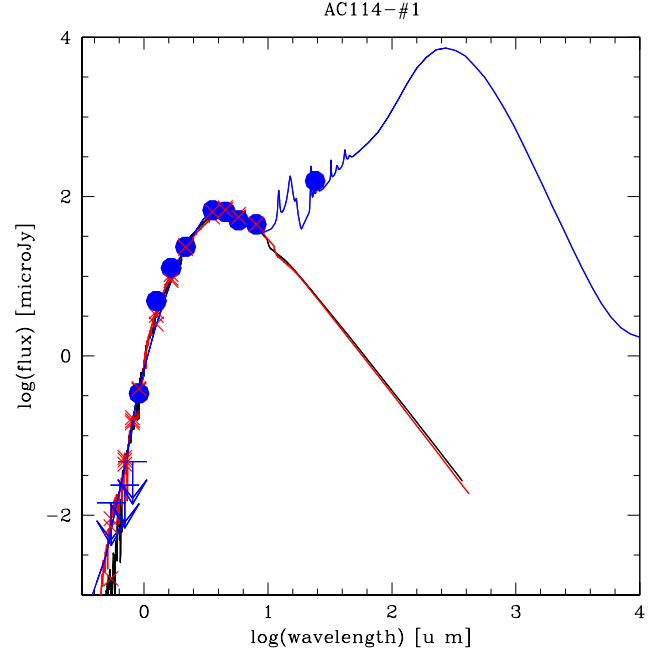


**Fig. 12.** AC114-#1: Best fit SEDs with Bruzual & Charlot templates (black line: burst of 4.5 Gyr age and  $A_V = 2.4$  at  $z = 1.3$ ), S04gyr templates (red: 1.0 Gyr,  $A_V = 2.8$ ,  $z = 1.6$ ), and with GRASIL templates (blue: M52 template +  $A_V = 3.8$ ,  $z = 1.0$ ). Note that by construction only the GRASIL templates include dust emission.

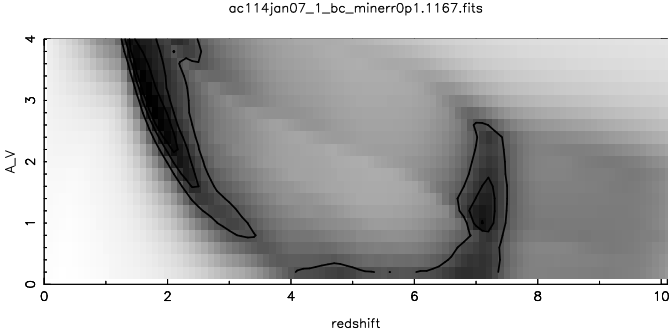


**Fig. 11.** Same as Fig. 2 for AC114-#1.

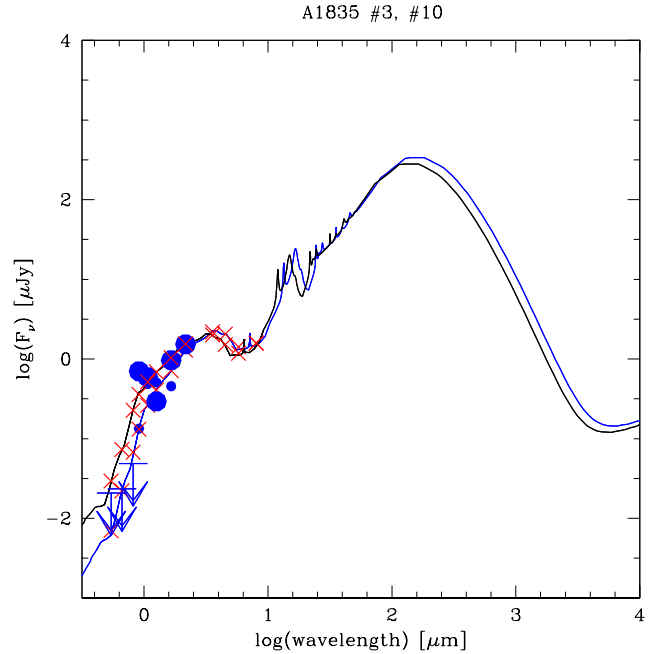


**Fig. 13.** Model fits for A1835 #3 (black) and #10 (blue) using GRASIL templates showing predictions for the Herschel/sub-mm/ALMA spectral domain.



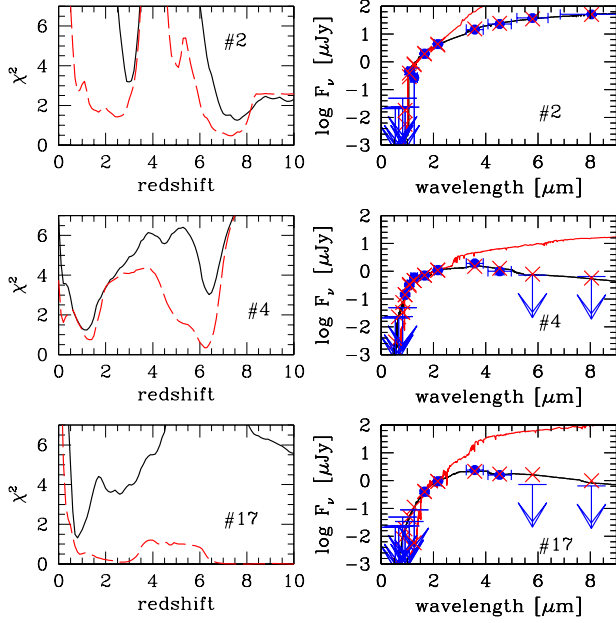


**Fig. 14.** Comparison of photometric redshifts derived with or without IRAC photometry for selected objects. **Left panels:**  $\chi^2$  of the best fitting template versus redshift obtained from SED fits including all the photometry (black solid lines), or obtained from SED fits excluding the IRAC photometric measurements (red dashed lines). **Right panels:** Best fit SED including all photometry (black solid curve) and excluding IRAC photometry (red solid). The observations are shown by the blue symbols. From top to bottom the objects are: A1835-#2, #4, and #17. These objects illustrate three typical behaviours: 1) degenerate/ambiguous low- and high- $z$  solutions even with IRAC photometry (#2, top panels), 2) degenerate/ambiguous low- and high- $z$  solutions whose degeneracy is lifted thanks to IRAC photometry (#4, middle panel), and 3) unconstrained photometric  $z$  from ground-based photometry, which becomes well defined low- $z$  solution with IRAC photometry (#17, bottom panel).

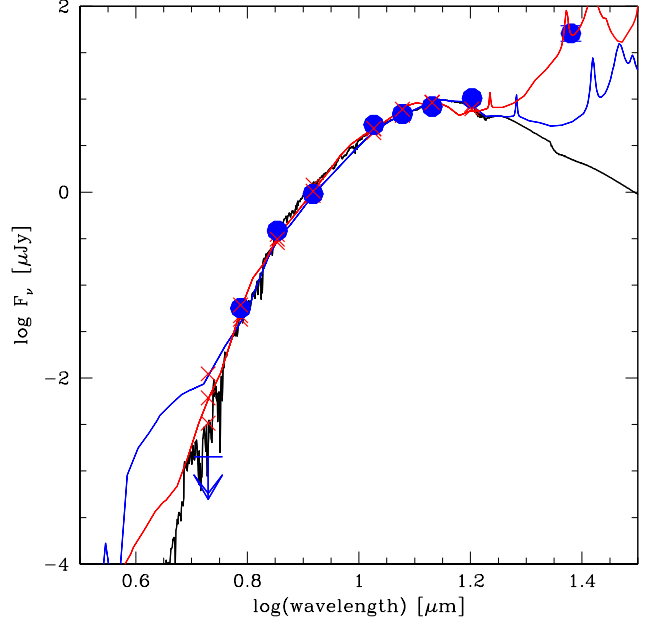


**Fig. 16.**  $z \sim 1.8$ – $2.6$  SED fits to the observations of HUDF-J2 from Mobasher et al. (2005). Black line: fit with BCCWW templates at  $z_{\text{fit}} = 2.59$ . Red: GRASIL M82 template and additional  $A_V = 2.8$  at  $z_{\text{fit}} \sim 1.8$ . Blue: GRASIL HR10 template without additional extinction at  $z_{\text{fit}} \sim 2.3$ .

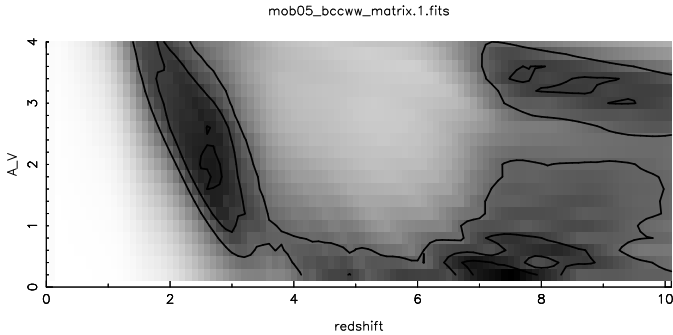


**Fig. 15.** Same as Fig. 2 for HUDF-J2. Formally the best fit is found at high redshift ( $z_{\text{fit}} \sim 6.4$ – $7.4$ ). However, for various reasons, including the  $24 \mu\text{m}$  flux and the exceptional luminosity of this object if at high  $z$ , we consider it more likely that this galaxy is at  $z \sim 2.4$ – $2.6$ . See discussion in text.

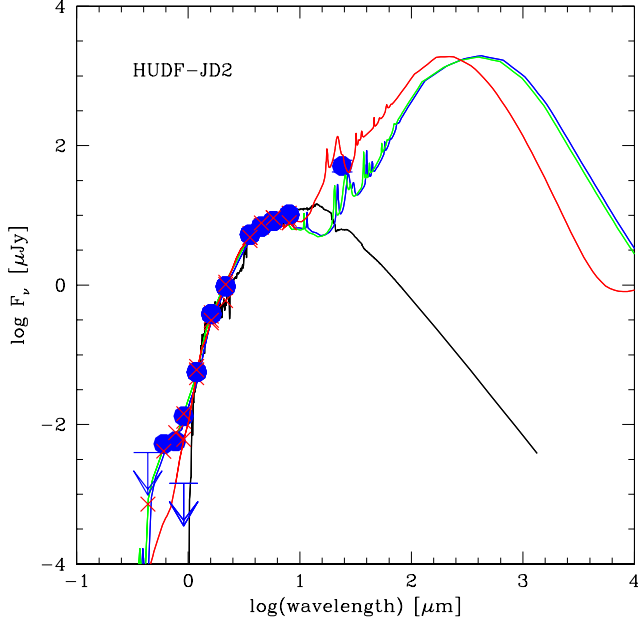


**Fig. 17.** SED fits to the observations of HUDF-J2. The near-IR and IRAC/Spitzer photometry is taken from Mobasher et al. (2005); in the optical we adopt either ((i) the  $z_{850LP}$  non-detection from Mobasher et al. (2005) or ((ii) the revisited photometry from Dunlop et al. (2006) yielding a  $B_{435}$  non-detection plus detections in  $V_{606}$ ,  $i_{775}$  and  $z_{850LP}$ ). Fitting ((i) with BCCWW templates yields a best fit at high- $z$  ( $z \sim 7.4$ , black line). Fitting ((i) with GRASIL templates, we obtain a best fit at  $z \sim 1.8$  with the M82 template and additional  $A_V = 2.8$  (red line) or at  $z \sim 2.3$  with the HR10 template (and no additional extinction; shown in blue). Adopting ((ii) the best fit with GRASIL templates is at  $z \sim 2.3$  with the HR10 template (and no additional extinction; shown in green). Note that all “low- $z$ ” solutions using GRASIL templates reproduce naturally the observed  $24 \mu\text{m}$  flux.